Fixed-time Rendezvous Control of Spacecraft with a Tumbling Target under Loss of Actuator Effectiveness

Boyan Jiang[1], Qinglei Hu[2] and Michael I. Friswell[3]

[1] Department of Control Science and Engineering, Harbin Institute of Technology, Harbin 150001, China

[2] School of Automation Science and Electrical Engineering, Beihang University, Beijing, 100191 China

[3]College of Engineering, Swansea University, Singleton Park, Swansea SA2 8PP, UK

Abstract: This paper investigates the fixed-time fault tolerant control problem of spacecraft rendezvous and docking with a freely tumbling target in the presence of external disturbance and thruster faults. More specifically, based on the attitude of the target spacecraft, a line-of-sight coordinate frame is defined first, and the dynamical equations relative to the tumbling target are derived to describe the relative position (not 6-DOF). Then two fixed-time position controllers are proposed to guarantee that the closed-loop system is stable in finite-time in the sense of a fixed-time concept, even in the presence of simultaneous external disturbance and thruster faults. Numerical simulations illustrate that the chaser spacecraft can successfully perform the rendezvous using the proposed controllers.

Index Terms—Spacecraft, fixed-time control, translation control, actuator faults, sliding mode control

1. Introduction

On-orbit servicing is a vital method to extend the lifetime and enhance the performance of spacecraft. Autonomous rendezvous and docking are the most important technology and have received attention from many researchers. However, there exist relatively few research results about approaching and docking with a (freely) tumbling target spacecraft. The classic examples are refueling a powerless spacecraft, repairing failed spacecraft, upgrading a flying satellite, removing space debris and so on. For example, when the Soviets lost

control of Salyut 7 and it drifted for months totally abandoned in 1985 [1]. The Soyuz T-13 carried the repair crew to rendezvous with the Salyut 7, and after two days they approached the Salyut. The cosmonauts discovered the station was in a slow roll (no more than three tenths of a degree per second) and its solar arrays pointed randomly. This is a practical example of a rendezvous with a tumbling target and there are many other similar cases. Such missions are desirable and significant for many expensive and important spacecraft, such as the Hubble Telescope and the International Space Station.

Significant advances have been made to perform relative translation in the area of rendezvous and docking in recent years. The C-W (Clohessy Wiltshire) equations [2] have been widely used to describe the linear relative motion between the chaser and target spacecraft. But the C-W equations are derived on the assumption that the target spacecraft flies on a circular orbit, and first-order approximations are used, where second and higher order terms in the relative positions and velocities are neglected. Moreover, many other improved relative dynamics models have been derived, such as the fully nonlinear C-W equations [3], the T-H (Tschauner-Hempel) equations [4], the line of sight (LOS) based equations [5-7] and others [8,9]. In the terminal phase of rendezvous and docking (within several hundred meters), the relative distance and angles of line of sight (LOS) are the most direct and important measurement data for an autonomic and chaser spacecraft [10], especially when the target is non-cooperative. Hence LOS coordinate frame based dynamical equations for the relative motion are useful and some achievements have been made in recent years. For example, Yu [5] derived the LOS coordinate frame based dynamical equations of two spacecraft when their orbits are coplanar. Yu [6,7] gave more complete dynamical equations in the LOS coordinate frame. However, all of the existing research results for the LOS coordinate frame only consider a class of static attitude targets, whose body-fixed coordinate frame is completely still relatively to its orbit coordinate frame; these results are not suitable for a tumbling target spacecraft.

With the development of advanced control theory, numerous advanced methods have been developed

to achieve the rendezvous control mission in recent years. For example, Gao et al. [11] investigated the problem of robust H_∞ techniques for a class of spacecraft rendezvous systems. Adaptive sliding mode control has been used to solve the rendezvous and docking problem [12]. Considering the position measurement errors and uncertain mass properties, Singla et al. [13] proposed an output feedback structured model reference adaptive controller for spacecraft rendezvous and docking problems. Note that both of these references used the fully nonlinear C-W equations in the synthesis of their controllers. Feedback and adaptive controllers have been proposed to solve the control problem of relative motion in the presence of uncertainties in the thruster alignments and chaser spacecraft's mass [14,15]. Zhang et al. [16] designed a guidance controller and used an artificial potential function guidance to ensure the target is approached safely.

However, all of the dynamical equations and controllers in above references do not consider the situation when the target spacecraft is tumbling/rotating. In fact, there are only a few research results about the control of rendezvous and docking with a tumbling target. Lu et al. [17] studied the problem of approaching and docking with a freely tumbling target and the designed integrated controller can ensure the docking device of the chaser spacecraft is always pointing to the tumbling target. Di Cairano et al. [18] proposed a Model Predictive Control approach to solve the problem of rendezvous and proximity maneuvering with a tumbling in an orbital plane. Liang et al. [19] and Michael et al. [20] presented two attitude controllers to enable the chaser spacecraft to rotate at the same angular velocity as the tumbling target spacecraft in their rendezvous and docking. Note that none of the dynamical equations in the above control system is based on the target's tumbling attitude. A tumbling target is difficult to model because both the position and attitude of the chaser and target spacecraft interact, and the controller design is also difficult because the dynamical and kinematic equations are highly nonlinear. As part contributions of our work, defining a coordinate frame based on the target's attitude and deriving dynamical equations relative to the tumbling target are necessary for rapidly and accurately performing the rendezvous.

Although there have been many research achievements for rendezvous and docking with a cooperative or a non-cooperative target, none of the existing control schemes are based on finite-time control theory. Finite-time control, which has a fast convergence rate, high precision control performance, and good disturbance rejection properties, is a new theory that has received increased attention of scholars in the last ten years. To state clearly the definition of finite-time stability, take example for PID controller, it is noted that the states of the PID control system can converge toward but never reach the equilibrium in a finite time. Benefited from one more homogeneity power tuning parameters, the finite-time controller have a faster convergence rate than PID controller, and the system sates can reach he equilibrium in a finite time. The most common finite-time control methods can be broadly classified into two categories: the homogeneous domination approach [21-22] and the Lyapunov based approach [23]. Unfortunately, the proof of convergence for the homogeneous approach is invalid when the system includes disturbances and uncertainties. Furthermore, the homogeneous approach cannot estimate the settling time. Hence Lyapunov based approaches have attracted most researcher interest recently, and some achievements have been made to solve the finite-time problem of spacecraft motion [24]. Furthermore, to employ the nice features of sliding mode control(SMC), such as better disturbance rejection property and better robustness against uncertainties, many researchers combine the concept of finite-time stability with SMC, and use terminal sliding mode controller(TSMC) in the spacecraft control system[25-26]. However, the initial value of the system state must be known to estimate the settling time by the existing Lyapunov based finite-time approaches. In view of that, Polyakov et al. proposed the concept of fixed-time stability, which can estimate the upper bound of settling time without the knowledge of the initial conditions[27-28]. Then Levant studied the relationship between finite-time stability and fixed-time stability [29]. In the initial design of spacecraft control system, it is desirable to predict the settling time independently initial conditions. So far, to the best of authors' knowledge, there is no fixed-time control result for spacecraft motion, which is the main contribution of this paper.

In actual spacecraft control systems, some catastrophic faults may occur due to malfunctions of the thrusters and other components. If the translation controller does not have any fault tolerance capability, severe performance degradation and system instability would result in rendezvous mission failure. The fault-tolerant control (FTC) strategies can be classified into two categories: active FTC and passive FTC. The active FTC approach is to respond to the failure by reconfiguring the remaining (often redundant) system elements based on real-time information from a fault detection and diagnosis (FDD) scheme. Numerous active FTC strategies have been studied for spacecraft missions in the past decades, for instance, the work of Chen et al. [30] and Patton et al. [31] about the Mars Express mission, the work reported in Fonood et al. [32-33] and Henry et al. [34] about the Mars Sample Return (MSR) mission, and the work of Henry [35] about the Microscope satellite. In contrast to active FTC approach, neither an FDD scheme nor a controller reconfiguration mechanism is needed in the passive approach. The passive method utilizes a single robust controller to deal with a certain well defined fault sets, and there also have been a great deal of results in the literature on spacecraft control, such as the work of Qian et al. [36] about the spacecraft rendezvous system, the work reported in Marwaha et al. [37] about the Mars entry vehicle and the work of Hu et al. [38-39] about the spacecraft attitude control. Both of active FTC and passive FTC have their respective advantages and limitations Even though the control objective of their methods are the same, each approach have its own unique ways to achieve the objective. Interested readers shall refer to the systematic studies of active and passive FTC strategies in references [40] and [41], for good surveys. In comparison with an active FTC, the passive FTC is more difficult to achieve optimal performance under any design basis fault condition. However, the passive FTC has the advantage of avoiding time delay introduced by the online FDD and controller reconfiguration in active FTC. Motivated by the above, in this paper, under considering actuator faults and transient performance requirements, new passive fault-tolerant controllers will be designed to perform the challenging rendezvous mission, and these are the main research targets in this work.

Inspired by the fixed-time stabilization concept, this paper investigates the fault tolerant control problem in rendezvous and docking with a freely tumbling target spacecraft, and two fixed-time controllers are developed. The first ensures that all of the system states converge to zero in a fixed time without considering external disturbances and actuator faults. The second can guarantee fixed-time reachability of the system states into the small neighborhood of the designed fixed-time sliding mode in the presence of actuator faults and external disturbances. The rest of this paper is organized as follows. Section 2 defines a LOS coordinate frame based on the target's attitude and derives dynamic equations for rendezvous and docking with a tumbling target. Section 3 describes the definition and lemmas that will be used for the relative motion controllers. In Sections 4 and 5, the fixed-time based sliding mode and fixed-time controllers are designed. Simulation results that demonstrate various features of the proposed controllers are given in Section 5, followed by conclusions and future work.

Notation: Throughout this paper, we use $\|\bullet\|$ for the Euclidean norm of vectors and the induced norm for matrices. For a given vector $\boldsymbol{x}=[x_1 \quad x_2 \quad x_3]^{\mathrm{T}} \in \mathrm{R}^3$, define $\boldsymbol{x}^{\alpha}=\left[x_1^{\alpha} \quad x_2^{\alpha} \quad x_3^{\alpha}\right]^{\mathrm{T}}$, $\operatorname{sgn}(\boldsymbol{x})=[\operatorname{sgn}(x_1) \quad \operatorname{sgn}(x_2) \quad \operatorname{sgn}(x_3)]^{\mathrm{T}}$, $sig(\boldsymbol{x})^{\alpha}=\left[|x_1|^{\alpha}\operatorname{sgn}(x_1) \quad |x_2|^{\alpha}\operatorname{sgn}(x_2) \quad |x_3|^{\alpha}\operatorname{sgn}(x_3)\right]^{\mathrm{T}}$, where $\alpha \in \mathrm{R}$, and $\operatorname{sgn}(\cdot)$ denotes the sign function.

2. Relative Equations of Kinematic

2.1 A LOS Coordinate Frame based on the Attitude of the Target

Before proposing the LOS coordinate frame, the following frequently used coordinate systems are defined.

(1) The Earth-centered inertial coordinate system is denoted as $Ox_Iy_Iz_I$ and is fixed to the center of the Earth. The Ox_I axis points toward the vernal equinox, the Oz_I axis extends through the North Pole, the Oy_I axis completes the triad.

(2) The body-fixed coordinate frame of the target spacecraft is denoted as $O_tx_ty_tz_t$ and is fixed to the

center of target spacecraft.

As shown in Fig. 1, $\vec{r}_t$ is the position vector from the Earth center to the target spacecraft, $\vec{r}_c$ is the position vector from the Earth center to the chaser spacecraft, and $\vec{\rho}$ is the relative position vector from the chaser spacecraft to the target. Define the relations $|\vec{r}_t| = r_t$, $|\vec{r}_c| = r_c$ and $|\vec{\rho}| = \rho$. The coordinate frame $O_c x_t y_t z_t$ is parallel to the target body-fixed coordinate frame $O_t x_t y_t z_t$. The relative position of the two spacecraft can be expressed as a set of spherical coordinates $[\rho, \theta, \psi]^{\mathrm{T}}$ in the LOS coordinate frame $O_c x_L y_L z_L$, where $O_c x_L$ points to the target from the chaser spacecraft, ρ is the relative distance, and $\theta \in (-\pi/2, \pi/2)$ and $\psi \in (-\pi, \pi)$ are the rotational angles needed to align the $O_c x_t$ axis with the line-of-sight by consecutive rotations about the $O_c y_t$ axis and then the $O_c z_L$ axis, respectively. That is to say, with the rotation sequence $\theta \to \psi$, $O_c x_t y_t z_t$ can be transformed to the LOS coordinate frame $O_c x_L y_L z_L$.

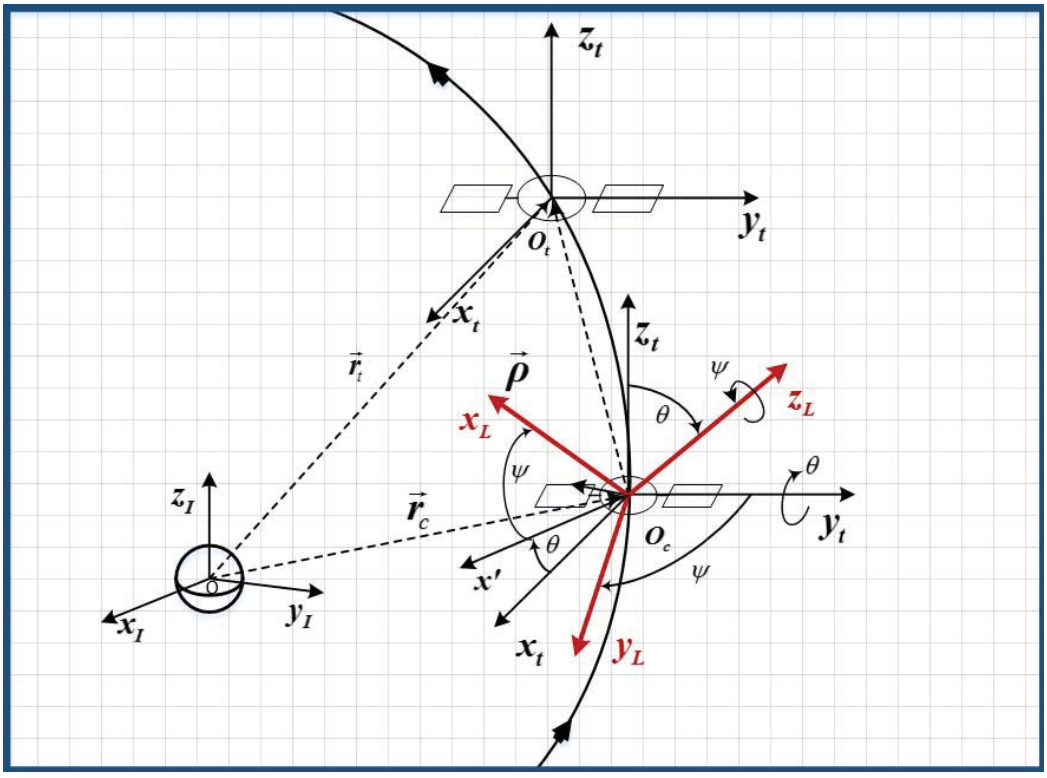

Fig. 1 The relation between the LOS coordinate frame and the attitude of the target

Remark 1. Compared with previous LOS coordinate frames[6-7, 14-16], the proposed LOS coordinate frame based on the attitude of the target is not only fixed to the center of the chaser spacecraft, but is also related

directly to the target's attitude. Thus, the proposed LOS coordinate frame has the advantages that: (1) it can be applied to a tumbling target and arbitrary orbital forms, and (2) the chaser spacecraft approaches the docking axis (i.e. the –X axis of the body-fixed Coordinate Frame of the target $O_t x_t y_t z_t$) of a tumbling target when the state variables in the LOS equations converge to the equilibrium point.

2.2 Equations of Kinematic in the Proposed LOS Coordinate Frame

In this section, the LOS based relative equation of kinematic between two spacecraft with spherical coordinates (ρ, θ, ψ) will be derived and discussed. By taking the second derivative of the relative position $\vec{\boldsymbol{\rho}} = \vec{\boldsymbol{r}}_t - \vec{\boldsymbol{r}}_c$ between two spacecraft in the Earth-centered inertial coordinate system, one has

$$\frac{d^2\vec{\boldsymbol{\rho}}}{dt^2} = \frac{d^2\vec{\boldsymbol{r}}_t}{dt^2} - \frac{d^2\vec{\boldsymbol{r}}_c}{dt^2} = \frac{\mu}{r_t^3}\left(-\vec{\boldsymbol{r}}_t + \frac{r_t^3}{r_c^3}\vec{\boldsymbol{r}}_c\right) + \vec{\boldsymbol{a}}_c + \vec{\boldsymbol{a}}_d\,, \qquad \vec{\boldsymbol{a}}_d = \vec{\boldsymbol{a}}_{J2c} - \vec{\boldsymbol{a}}_{J2t} + \vec{\boldsymbol{a}}_w \tag{1}$$

$$\vec{\boldsymbol{a}}_{J2i}\big|_I = -\frac{3}{2}J_2\frac{\mu R_e^2}{r_i^5}\left[\left(X - \frac{5Z^2X}{r_i^2}\right)\ \left(Y - \frac{5Z^2Y}{r_i^2}\right)\ \left(3Z - \frac{5Z^3}{r_i^2}\right)\right]^{\mathrm{T}} \qquad i = c\ or\ t \tag{2}$$

where μ is the standard gravitational parameter and $\vec{\boldsymbol{a}}_c$ denotes the chaser spacecraft's control acceleration from thrust force. The derivative with a subscript "I" means that the derivative is in the inertial frame (I-frame). If the orbit is circular, $\vec{\boldsymbol{a}}_{J2i}$ denotes the earth non-spherical perturbation, for both vehicles ($\vec{\boldsymbol{a}}_{J2c}$ for the chaser and $\vec{\boldsymbol{a}}_{J2t}$ for the target) caused by the Earth's oblateness, or equatorial bulge and J2 is the first zonal coefficient terms in the Legendre polynomial[42-43].The X, Y and Z in Eq.(2) denote the spacecraft's positon in the inertial frame. $\vec{\boldsymbol{a}}_w$ is considered to be small acceleration due to the atmospheric drag, the gravity fields of other planet, solar pressure or venting which also perturbs the spacecraft's motion. The small accelerations are grouped together because they have slighter significant effect of spacecraft orbits than the earth non-spherical perturbation.

From the cosine law, under the assumption $\frac{\rho}{r_t} << 1$, the distance between the chaser spacecraft and the center of the Earth can be approximated as

$$r_c^2 = \rho^2 + r_t^2 - 2\rho r_t \cos\left(\angle O_c O_t O\right) = \rho^2 + r_t^2 - 2\vec{\boldsymbol{\rho}} \cdot \vec{\boldsymbol{r}}_t \approx r_t^2 \left(1 - \frac{2\vec{\boldsymbol{\rho}} \cdot \vec{\boldsymbol{r}}_t}{r_t^2}\right)$$
$$r_c = r_t \left(1 - \frac{2\vec{\boldsymbol{\rho}} \cdot \vec{\boldsymbol{r}}_t}{r_t^2}\right)^{1/2} \tag{3}$$

where the notation $\cos(\angle \mathrm{O}_c\mathrm{O}_t\mathrm{O})$ denotes the cosine of the angle $\cos(\angle \mathrm{O}_c\mathrm{O}_t\mathrm{O})$, and definition of the angle $\cos(\angle \mathrm{O}_c\mathrm{O}_t\mathrm{O})$ can be find in the Fig. 1.

Using the Maclaurin expansion $(1+a)^{-3/2} = 1 - \frac{3}{2}a + \frac{15}{8}a^2 + \cdots$,

$$\frac{1}{r_c^3} \approx \frac{1}{r_t^3}\left(1 + \frac{3\vec{\boldsymbol{\rho}} \cdot \vec{\boldsymbol{r}}_t}{r_t^2}\right) \tag{4}$$

Then, substituting Eq.(4) into Eq.(1) yields

$$\frac{d^2\vec{\boldsymbol{\rho}}}{dt^2} = \frac{\mu}{r_t^3}\left[-\vec{\boldsymbol{r}}_t + \left(1 + \frac{3\vec{\boldsymbol{\rho}} \cdot \vec{\boldsymbol{r}}_t}{r_t^2}\right)\vec{\boldsymbol{r}}_c\right] + \vec{\boldsymbol{a}}_c + \vec{\boldsymbol{a}}_d \approx \frac{\mu}{r_t^3}\left(-\vec{\boldsymbol{\rho}} + \frac{3\vec{\boldsymbol{\rho}} \cdot \vec{\boldsymbol{r}}_t}{r_t^2}\vec{\boldsymbol{r}}_t\right) + \vec{\boldsymbol{a}}_c + \vec{\boldsymbol{a}}_d \tag{5}$$

Note that vectors $\vec{\boldsymbol{\rho}}$ and $\vec{\boldsymbol{r}}_t$ can be expressed as $\boldsymbol{\rho} = [\rho, 0, 0]^{\mathrm{T}} \in \mathrm{R}^3$ and $\boldsymbol{r}_t = \boldsymbol{R}_{Lt}\boldsymbol{R}_{tI}\boldsymbol{R}_{IO}[r_t, 0, 0]^{\mathrm{T}} \in \mathrm{R}^3$ in the LOS coordinate frame, where $\boldsymbol{R}_{Lt} = \begin{bmatrix} \cos\psi\cos\theta & \sin\psi & -\cos\psi\sin\theta \\ -\sin\psi\cos\theta & \cos\psi & \sin\psi\sin\theta \\ \sin\theta & 0 & \cos\theta \end{bmatrix}$ is the coordinate transformation from the target body-fixed frame to the LOS frame, $\boldsymbol{R}_{tI} = \left(q_{t0}^2 - \boldsymbol{q}_t^{\mathrm{T}}\boldsymbol{q}_t\right)\mathrm{I}_3 + 2\boldsymbol{q}_t\boldsymbol{q}_t^{\mathrm{T}} - 2q_{t0}[\boldsymbol{q}_t^{\times}]$ is the coordinate transformation from the Earth-centered inertial coordinate frame to the target body-fixed coordinate frame, and

$\boldsymbol{R}_{IO} = \begin{bmatrix} \cos(\omega_0 + f) & \sin(\omega_0 + f) & 0 \\ -\sin(\omega_0 + f) & \cos(\omega_0 + f) & 0 \\ 0 & 0 & 1 \end{bmatrix}\begin{bmatrix} 1 & 0 & 0 \\ 0 & \cos i_0 & \sin i_0 \\ 0 & -\sin i_0 & \cos i_0 \end{bmatrix}\begin{bmatrix} \cos(\Omega) & \sin(\Omega) & 0 \\ -\sin(\Omega) & \cos(\Omega) & 0 \\ 0 & 0 & 1 \end{bmatrix}$ is the coordinate transformation from the orbital coordinate frame to the Earth-centered inertial coordinate frame. Note that, for any vector $\boldsymbol{a} = [a_1, a_2, a_3]^{\mathrm{T}}$, the notation $\boldsymbol{a}^{\times}$ is used to denote the skew-symmetric matrix $\boldsymbol{a}^{\times} = \begin{bmatrix} 0 & -a_3 & a_2 \\ a_3 & 0 & -a_1 \\ -a_2 & a_1 & 0 \end{bmatrix}$. In addition, $[q_{t0}, \boldsymbol{q}_t^{\mathrm{T}}]^{\mathrm{T}} \in \mathrm{R}^4$ is the attitude quaternion of the target spacecraft, and ω_0, f, i_0 and Ω are the argument of perigee, the true anomaly, the orbit inclination, and the right ascension of the ascending node of the target spacecraft, respectively. Note that that all of the information relating to the target spacecraft's attitude and orbit are required before rendezvous and docking. To this end, the Eq.(5) can be

re-written in the LOS frame as

$$\left.\frac{d^2\vec{\boldsymbol{\rho}}}{dt^2}\right|_L = \frac{\mu}{r_t^3}\left(-\boldsymbol{\rho} + \frac{3\boldsymbol{\rho}\cdot\mathbf{r}_t}{r_t^2}\mathbf{r}_t\right) + \mathbf{a}_c + \mathbf{a}_d \tag{6}$$

where $\boldsymbol{\rho} \in \mathrm{R}^3$, $\mathbf{a}_c \in \mathrm{R}^3$ and $\mathbf{a}_d \in \mathrm{R}^3$ are the vectors $\vec{\boldsymbol{\rho}}$, $\vec{\mathbf{a}}_c$ and $\vec{\mathbf{a}}_d$ expressed in the LOS frame, respectively. The derivative with a subscript "L" means that the derivative is in the LOS frame.

If $\dot{\boldsymbol{\rho}}$ and $\ddot{\boldsymbol{\rho}}$ are denoted as the first and second derivative of $\boldsymbol{\rho}$ in the LOS frame, one has

$$\left.\frac{d\vec{\boldsymbol{\rho}}}{dt}\right|_L = \dot{\boldsymbol{\rho}} + \boldsymbol{\omega}_L \times \boldsymbol{\rho} \tag{7}$$

$$\left.\frac{d^2\vec{\boldsymbol{\rho}}}{dt^2}\right|_L = \ddot{\boldsymbol{\rho}} + 2\boldsymbol{\omega}_L \times \dot{\boldsymbol{\rho}} + \dot{\boldsymbol{\omega}}_L \times \boldsymbol{\rho} + \boldsymbol{\omega}_L \times \left(\boldsymbol{\omega}_L \times \boldsymbol{\rho}\right) \tag{8}$$

where $\boldsymbol{\omega}_L = \mathbf{R}_{Lt}\boldsymbol{\omega}_t + \begin{bmatrix}\dot{\theta}\sin\psi & \dot{\theta}\cos\psi & \dot{\psi}\end{bmatrix}^{\mathrm{T}} \in \mathrm{R}^3$ denotes the angular velocity of the LOS frame with respect to the Earth-centered inertial frame expressed in the LOS frame, and $\boldsymbol{\omega}_t \in \mathrm{R}^3$ denotes the body-fixed reference frame of the target spacecraft with respect to an Earth-centered inertial frame expressed in the body-fixed reference frame. Furthermore, the first derivative of $\boldsymbol{\omega}_L$ in the LOS frame and $\boldsymbol{\omega}_t$ in the body-fixed reference frame of the target spacecraft can be written as, respectively,

$$\dot{\boldsymbol{\omega}}_L = \dot{\mathbf{R}}_{Lt}\boldsymbol{\omega}_t + \mathbf{R}_{Lt}\dot{\boldsymbol{\omega}}_t + \begin{bmatrix}\ddot{\theta}\sin\psi + \dot{\theta}\dot{\psi}\cos\psi & \ddot{\theta}\cos\psi - \dot{\theta}\dot{\psi}\sin\psi & \ddot{\psi}\end{bmatrix}^{\mathrm{T}} \tag{9}$$

$$\dot{\boldsymbol{\omega}}_t = -\mathbf{J}_t^{-1}\boldsymbol{\omega}_t^{\times}\mathbf{J}_t\boldsymbol{\omega}_t + \mathbf{J}_t^{-1}\boldsymbol{\tau}_t + \mathbf{J}_t^{-1}\mathbf{d}_t \tag{10}$$

where $\mathbf{J}_t = \mathbf{J}_t^{\mathrm{T}} \in \mathrm{R}^{3\times3}$ denotes the positive definite inertia matrix of the target spacecraft, $\boldsymbol{\tau}_t \in \mathrm{R}^3$ denotes the vector of control torques commanded by the attitude controller of the target spacecraft in the body-fixed reference frame., and $\mathbf{d}_t \in \mathrm{R}^3$ denotes the target's external disturbance torque vector induced from the environment, and includes environmental torques such as the gravitational torque and the torque arising from the aerodynamic drag, solar radiation, and magnetic effects, in the body-fixed reference frame.

From Eqs. (6) and (8), one has

$$\frac{\mu}{r_t^3}\left(-\boldsymbol{\rho} + \frac{3\boldsymbol{\rho}\cdot\mathbf{r}_t}{r_t^2}\mathbf{r}_t\right) + \mathbf{a}_c + \mathbf{a}_d = \ddot{\boldsymbol{\rho}} + 2\boldsymbol{\omega}_L \times \dot{\boldsymbol{\rho}} + \dot{\boldsymbol{\omega}}_L \times \boldsymbol{\rho} + \boldsymbol{\omega}_L \times \left(\boldsymbol{\omega}_L \times \boldsymbol{\rho}\right) \tag{11}$$

Again, substituting Eq.(9) and Eq.(10) into Eq.(11) and multiplying both side of Eq.(11) by the mass, m_c, of

the chaser spacecraft yields

$$\boldsymbol{A}_1\ddot{\bar{\boldsymbol{x}}}+\boldsymbol{B}_1=\boldsymbol{F}_L+\boldsymbol{d}_L-m_c\boldsymbol{R}_{Lt}\boldsymbol{J}_t^{-1}\boldsymbol{\tau}_t\times\boldsymbol{\rho} \tag{12}$$

$$\boldsymbol{d}_L=-m_c\boldsymbol{R}_{Lt}\boldsymbol{J}_t^{-1}\boldsymbol{d}_t\times\boldsymbol{\rho}-m_c\boldsymbol{a}_d \tag{13}$$

where $\boldsymbol{B}_1=\begin{bmatrix}0\\0\\m_c\rho\dot{\theta}\dot{\psi}\sin\psi\end{bmatrix}+2m_c\boldsymbol{\omega}_L\times\dot{\boldsymbol{\rho}}+m_c\left(\dot{\boldsymbol{R}}_{Lt}\boldsymbol{\omega}_t-\boldsymbol{R}_{Lt}\boldsymbol{J}_t^{-1}\boldsymbol{\omega}_t^{\times}\boldsymbol{J}_t\boldsymbol{\omega}_t\right)\times\boldsymbol{\rho}+m_c\boldsymbol{\omega}_L\times\left(\boldsymbol{\omega}_L\times\boldsymbol{\rho}\right)+\frac{\mu m_c}{r_t^3}\left(\boldsymbol{\rho}-\frac{3\boldsymbol{\rho}\cdot\boldsymbol{r}_t}{r_t^2}\boldsymbol{r}_t\right)$,

$\bar{\boldsymbol{x}}=\begin{bmatrix}\rho & \psi & \theta\end{bmatrix}^{\mathrm{T}}$, $\boldsymbol{A}_1=m_c\begin{bmatrix}1&0&0\\0&\rho&0\\0&0&-\rho\cos\psi\end{bmatrix}$, $\boldsymbol{F}_L$ is the control vector produced by the thrusters in the LOS coordinate frame, and $\boldsymbol{d}_L$ is the orbital disturbance force of the two spacecraft.

In practice the docking position is not at the center of the spacecraft, so the relative position of the two spacecraft, ρ, should not tend to zero during rendezvous and docking. Let ρ_d be the desired distance and ρ_e be the relative position error, and $\rho=\rho_e+\rho_d$. Then, with the assumption that ρ_d is a constant with $\boldsymbol{\rho}_d=\begin{bmatrix}\rho_d & 0 & 0\end{bmatrix}^{\mathrm{T}}$ in the LOS coordinate frame, Eq.(12) can be re-written as

$$\boldsymbol{A}_2\ddot{\boldsymbol{x}}+\boldsymbol{B}_2=\boldsymbol{F}_L+\boldsymbol{d}_L-m_c\boldsymbol{R}_{Lt}\left(\boldsymbol{J}_t^{-1}\boldsymbol{\tau}_t+\boldsymbol{J}_t^{-1}\boldsymbol{d}_t\right)\times\left(\boldsymbol{\rho}_e+\boldsymbol{\rho}_d\right) \tag{14}$$

with the new state vector $\boldsymbol{x}=\begin{bmatrix}\rho_e,\psi,\theta\end{bmatrix}^{\mathrm{T}}$, and the new matrices $\boldsymbol{A}_2$ and $\boldsymbol{B}_2$ are given as

$$\boldsymbol{A}_2=m_c\begin{bmatrix}1&0&0\\0&\rho_e+\rho_d&0\\0&0&-\left(\rho_e+\rho_d\right)\cos\psi\end{bmatrix}$$

$$\boldsymbol{B}_2=m_c\begin{bmatrix}0 & 0 & \left(\rho_e+\rho_d\right)\dot{\theta}\dot{\psi}\sin\psi\end{bmatrix}^{\mathrm{T}}+2m_c\boldsymbol{\omega}_L\times\dot{\boldsymbol{\rho}}_e+m_c\left(\dot{\boldsymbol{R}}_{Lt}\boldsymbol{\omega}_t-\boldsymbol{R}_{Lt}\boldsymbol{J}_t^{-1}\boldsymbol{\omega}_t^{\times}\boldsymbol{J}_t\boldsymbol{\omega}_t\right)\times\left(\boldsymbol{\rho}_e+\boldsymbol{\rho}_d\right)$$
$$+m_c\boldsymbol{\omega}_L\times\left[\boldsymbol{\omega}_L\times\left(\boldsymbol{\rho}_e+\boldsymbol{\rho}_d\right)\right]+\frac{\mu m_c}{r_t^3}\left(\boldsymbol{\rho}_e+\boldsymbol{\rho}_d-\frac{3\left(\boldsymbol{\rho}_e+\boldsymbol{\rho}_d\right)\cdot\boldsymbol{r}_t}{r_t^2}\boldsymbol{r}_t\right)$$

The model of the spacecraft mass depends on the chosen thrusters. In this paper, electronic ION thrusters and chemical thrusters are considered. Assume there are *n* thrusters in the chaser spacecraft, and the *i* th thruster generates a force of F_{Si}. Then the mass flow is governed by

$$\dot{m}_c=-\sum_{i=1}^{n}\left[\left|F_{ci}\right|/\left(I_{sp}g\right)\right] \tag{15}$$

where $g = \mu / r_s^2$ is the time varying gravitation constant and I_{sp} is a characteristic of the chemical propellant used in the thruster[44].

Remark 2. Although the derivation above shares similar approximations with those in Ref. [15], the definition of the LOS coordinate frame are different in nature. In this work, the LOS based equations, (12) and (14), not only explicitly consider the target's attitude, but also the external disturbance and the attitude control torque of the target spacecraft. Thus, the main research objective of this paper is to target a certain class of tumbling spacecraft.

Remark 3. Equations (12) and (14) explicitly include the target's control torque, $\boldsymbol{\tau}_t$. If $\boldsymbol{\tau}_t = 0$, then Eqs. (12) and (14) can be applied to the rendezvous of a freely tumbling spacecraft. Furthermore, if the initial angular velocity and attitude quaternions of the target, and also the disturbance, are set to zero, i.e. $\boldsymbol{\omega}_t(0) = 0$, $\boldsymbol{q}_t(0) = 0$ and $\boldsymbol{d}_L = \boldsymbol{d}_t = 0$, then the equations are identical to those in Ref. [15]. In addition, if the target spacecraft is completely non-cooperative, which means $\boldsymbol{\omega}_t$ and $\dot{\boldsymbol{\omega}}_t$ are unknown, then observers should be designed to estimate $\boldsymbol{\omega}_t$ and $\dot{\boldsymbol{\omega}}_t$ of the target; this is beyond the scope of this paper.

3. Definitions and Lemmas

Consider the system

$$\dot{\boldsymbol{x}}(t) = \boldsymbol{f}(\boldsymbol{x}(t)), \quad \boldsymbol{x}(0) = \boldsymbol{0}, \quad \boldsymbol{f}(\boldsymbol{0}) = \boldsymbol{0}, \quad \boldsymbol{x} \in \mathrm{R}^n \tag{16}$$

where $\boldsymbol{f} : U_0 \to \mathrm{R}^n$ is continuous in an open neighborhood U_0 of the origin. Suppose that the system in Eq.(16) possesses a unique solution in forward time for all initial conditions.

Definition 1 (Ref. [27]). The equilibrium $\boldsymbol{x} = \boldsymbol{0}$ of the system in Eq.(16) is fixed-time stable if it is globally finite-time stable and the settling-time function $T(\boldsymbol{x})$ is bounded, i.e., existing positive constant $T_{\max}$ such that $T(\boldsymbol{x}) \le T_{\max}$, for any $\boldsymbol{x} \in \mathrm{R}^n$.

Lemma 1 (Ref. [27]). Consider the system in Eq.(16). Suppose there is a Lyapunov function $V(x)$

defined on a neighborhood $U \subset \mathrm{R}^n$ of the origin, and $\dot{V}(\boldsymbol{x}) \le -(\alpha V(\boldsymbol{x})^p + \beta V(\boldsymbol{x})^g)^k$, where $\alpha, \beta, p, g, k \in \mathrm{R}^+$, $pk < 1$ and $gk > 1$. Then the origin of the system in Eq.(16) is fixed-time stable, and any $V(\boldsymbol{x})$ that starts from U can reach $V(\boldsymbol{x}) \equiv 0$ in a fixed time. According to Definition 2, the settling time T of a fixed-time stable system is bounded and its bound is independent of the initial value of system states. Thus, we can conservatively estimate T as

$$T \le \frac{1}{\alpha^k (1-pk)} + \frac{1}{\beta^k (gk-1)} \tag{17}$$

without any knowledge of the initial value $V(\boldsymbol{x}_0)$.

Lemma 2 (Ref. [45]). Consider the nonlinear system in Eq.(16). Suppose that there exist a Lyapunov function $V(\boldsymbol{x})$, scalars $\alpha \in \mathrm{R}^+$, $p \in (0,1)$ and $0 < \vartheta < \infty$, such that $\dot{V}(\boldsymbol{x}) \le -\alpha V(\boldsymbol{x})^p + \vartheta$. Then, the trajectory of this system is practical finite-time stable. Moreover, the residual set of the solution of system (16) is given by $\left\{ \lim_{t \to T} \boldsymbol{x} \middle| V(\boldsymbol{x}) \le \left[\frac{\vartheta}{\alpha(1-\theta)} \right]^{\frac{1}{p}} \right\}$, where θ is a scalar and satisfies $0 < \theta \le 1$. And the time, T, needed to reach the residual set is bounded by $T \le \frac{V(x_0)^{1-p}}{\alpha\theta(1-p)}$, where $V(\boldsymbol{x}_0)$ is the initial value of $V(\boldsymbol{x})$.

Proposition 1. Consider the nonlinear system in Eq.(16). Suppose that there exist a Lyapunov function $V(\boldsymbol{x})$, scalars $\alpha, \beta, p, q, k \in \mathrm{R}^+$, $pk < 1$, $gk > 1$ and $0 < \vartheta < \infty$, such that $\dot{V}(\boldsymbol{x}) \le -(\alpha V(\boldsymbol{x})^p + \beta V(\boldsymbol{x})^g)^k + \vartheta$. Then, the trajectory of this system is practical fixed-time stable. Moreover, the residual set of the solution of system (16) is given by $\left\{ \lim_{t \to T} \boldsymbol{x} \middle| V(\boldsymbol{x}) \le \min\left\{ \alpha^{-1/p} \left(\frac{\vartheta}{1-\theta^k} \right)^{\frac{1}{kp}}, \beta^{-1/p} \left(\frac{\vartheta}{1-\theta^k} \right)^{\frac{1}{kg}} \right\} \right\}$, where θ is a scalar and satisfies $0 < \theta \le 1$. And the time, T, needed to reach the residual set is bounded by $T \le \frac{1}{\alpha^k \theta^k (1-pk)} + \frac{1}{\beta^k \theta^k (gk-1)}$.

Proof: the Proposition 1 can be easily proved based on Lemma 2, so we omit the proof here.

Lemma 3 (Ref. [23]). Consider the system in Eq.(16). Suppose there is a Lyapunov function $V(\boldsymbol{x})$,

scalars $p \in (0,1)$ and $\alpha \in \mathrm{R}^+$, such that $\dot{V}(\boldsymbol{x}) + \alpha V(\boldsymbol{x})^p < 0$. Then the origin of Eq.(16) is finite-time stable, and the settling time is given by $T \le \frac{1}{\alpha(1-p)} \left| V(x_0) \right|^{1-p}$, where $V(x_0)$ is the initial value of $V(\boldsymbol{x})$.

Lemma 4 (Ref. [46]). For any $\boldsymbol{x} \in \mathrm{R}^n$ and $a \in \mathrm{R}$, we have $\frac{\mathrm{d}|\boldsymbol{x}|^{a+1}}{\mathrm{d}t} = (a+1)\mathrm{diag}\left(\mathrm{sig}(\boldsymbol{x})^a\right)\dot{\boldsymbol{x}}$ and $\frac{\mathrm{d}\mathrm{sig}(\boldsymbol{x})^{a+1}}{\mathrm{d}t} = (a+1)\mathrm{diag}\left(|\boldsymbol{x}|^a\right)\dot{\boldsymbol{x}}$.

Lemma 5 (Ref. [47]). For any $x_i \in \mathrm{R}$, $i = 1,2....,n$, $\left(\sum_{i=1}^{n} |x_i|\right)^v \le \sum_{i=1}^{n} |x_i|^v$, where v is a real number and $v \in (0,1]$.

Lemma 6 (Ref. [48]). If v is a real number and $v > 1$, then for any $x \in \mathrm{R}$ and $y \in \mathrm{R}$, we have $|x+y|^v \le 2^{v-1} \left| x^v + y^v \right|$.

Proposition 2. If v is a real number and $v > 1$, then for any $x, y, z \in \mathrm{R}$ we have $|x+y+z|^v \le 2^{2v-2} \left| x^v + y^v + z^v \right|$.

Proof: the Proposition 2 can be easily proved based on Lemma 6, so we omit the proof here.

4. A New Fixed-time Sliding Mode Surface Design and Convergence Analysis

In this section, a new fixed-time sliding mode (SM) surface will be proposed for the problem of spacecraft rendezvous. In terms of the spherical coordinate $\boldsymbol{x} = [\boldsymbol{\rho_e}, \psi, \theta]^{\mathrm{T}}$, the new fixed-time SM is

$$\boldsymbol{S} = \dot{\boldsymbol{x}} + sig\left(\boldsymbol{\alpha_1} sig(\boldsymbol{x})^{p_1} + \boldsymbol{\beta_1} sig(\boldsymbol{x})^{g_1}\right)^{k_1} \tag{18}$$

where $\boldsymbol{\alpha_1} \in \mathrm{diag}(\alpha_{1i})$, $\boldsymbol{\beta_1} \in \mathrm{diag}(\beta_{1i})$, $i = 1,2,3$, $\alpha_{1i}, \beta_{1i}, p_1, g_1, k_1 > 0$, $p_1 k_1 \in (0,1)$ and $g_1 k_1 > 1$ are the free design parameters chosen by the designer. Then the following statements can be concluded.

Theorem 1. Consider the LOS-based equation of relative motion, Eq.(14), for the fixed-time SM, Eq.(18), satisfying $\boldsymbol{S} = \boldsymbol{0}$ under the Assumptions 1 and 2. Then $\boldsymbol{x} = \boldsymbol{0}$ and $\dot{\boldsymbol{x}} = \boldsymbol{0}$ can be reached in fixed-time T_x, even without requiring any knowledge of the initial and instantaneous values of the system states. The fixed-time T_x then satisfies

$$T_x \le \frac{1}{\lambda_{\min}\left(\boldsymbol{\alpha}_1\right)^{k_1} (1 - p_1 k_1)} + \frac{1}{\lambda_{\min}\left(\boldsymbol{\beta}_1\right)^{k_1} (g_1 k_1 - 1)} \tag{19}$$

Proof: If the sliding motion occurs for system (14), such that $\boldsymbol{q}$ and $\boldsymbol{\omega}$ remain on the fixed-time SM for all time, then we have $\boldsymbol{S}=\boldsymbol{0}$. Thus

$$\dot{\boldsymbol{x}}=-sig\left(\boldsymbol{\alpha_1}sig(\boldsymbol{x})^{p_1}+\boldsymbol{\beta_1}sig(\boldsymbol{x})^{g_1}\right)^{k_1} \tag{20}$$

Let the positive definite Lyapunov function be of the form $V_{xi}=|x_i|$, where $i=1,2,3$ and $\boldsymbol{x}=\left[x_1,x_2,x_3\right]^{\mathrm{T}}$.

Taking the derivative of V_{xi} along Eq.(20) yields

$$\begin{aligned}\dot{V}_{xi}&=\operatorname{sign}(x_i)\dot{x}_i=-\operatorname{sign}(x_i)\left|\alpha_{1i}sig(x_i)^{p_1}+\beta_{1i}sig(x_i)^{g_1}\right|^{k_1}\operatorname{sign}(\alpha_{1i}sig(x_i)^{p_1}+\beta_{1i}sig(x_i)^{g_1})\\&=-\left|\alpha_{1i}sig(x_i)^{p_1}+\beta_{1i}sig(x_i)^{g_1}\right|^{k_1}=-\left|\alpha_{1i}|x_i|^{p_1}+\beta_{1i}|x_i|^{g_1}\right|^{k_1}=-\left(\alpha_{1i}V_{xi}{}^{p_1}+\beta_{1i}V_{xi}{}^{g_1}\right)^{k_1}\end{aligned} \tag{21}$$

From Lemma 1, it can be concluded that the relative position errors (ρ_e,ψ,θ) are stabilized in finite time T_x, given by $T_x\le\dfrac{1}{\lambda_{\min}\left(\boldsymbol{\alpha}_1\right)^{k_1}(1-p_1k_1)}+\dfrac{1}{\lambda_{\min}\left(\boldsymbol{\beta}_1\right)^{k_1}(g_1k_1-1)}$, where $\lambda_{\min}(\bullet)$ represents the minimum eigenvalue of a given matrix. This shows that the bound of the convergence time T_x can be estimated even if we have no knowledge of the initial and instantaneous values of the system states.

5. Fixed-time Controller Design for Rendezvous and Docking with a Freely Tumbling Target

The problem of rendezvous and docking is studied for a non-cooperative target, which is out of control with no external disturbances (i.e. $\boldsymbol{\tau_t}$ and $\boldsymbol{d_t}$ in Eq.(14) equal zero), and is tumbling freely in space. The LOS based equation of relative motion in Eq.(14), incorporating thruster faults, can be combined to give

$$\boldsymbol{A}_2\ddot{\boldsymbol{x}}+\boldsymbol{B}_2=\boldsymbol{R}_{\boldsymbol{Lc}}\boldsymbol{D}\left(\boldsymbol{I}-\boldsymbol{E}\right)\boldsymbol{F}_{\boldsymbol{C}}+\boldsymbol{R}_{\boldsymbol{Lc}}\boldsymbol{D}\boldsymbol{E}\bar{\boldsymbol{F}}_{\boldsymbol{C}}+\boldsymbol{d}_{\boldsymbol{L}} \tag{22}$$

where $\boldsymbol{D}\in R^{3\times m}$ is the thruster configuration matrix, and m is the number of thrusters. $\boldsymbol{F_C}$ denotes the desired control force produced by the thrusters in the body-fixed coordinate frame of the chaser spacecraft. $\boldsymbol{I}$ represents the identity matrix with the appropriate dimensions. $\boldsymbol{E}=\operatorname{diag}(E_1,E_2\ldots E_m)\in\mathrm{R}^{m\times m}$ and E_i is the failure indicator for the i^{th} thruster pair. Note that the case $E_i=0$ means that the i^{th} thruster pair works normally; if $E_i=1$, the i^{th} thruster pair has failed completely; and $E_i\in(0,1)$ corresponds the case in which the i^{th} thruster pair has partially lost its effectiveness, but still works all of the time. $\bar{\boldsymbol{F}}_{\boldsymbol{C}}\in\mathrm{R}^m$ represents a stuck fault for the thruster [49].

The presented fault model in Eq.(22) can represent outage, loss of effectiveness, and stuck faults. $\boldsymbol{R}_{Lc} = \boldsymbol{R}_{Lt}\boldsymbol{R}_{tI}\boldsymbol{R}_{Ic}$ denotes the coordinate transformation from the body-fixed coordinate frame of the chaser spacecraft to the LOS frame, and $\boldsymbol{R}_{Ic}$ represents the coordinate transformation from the body-fixed coordinate frame of the chaser spacecraft to the Earth-centered inertial frame, and obtained in a similar way to $\boldsymbol{R}_{tI}$ and is directly related to the attitude of the chaser spacecraft.

To design the control scheme, the following reasonable assumption is required.

Assumption 1. The NAV is assumed to be perfect and the state and output noises are not taken into consideration.

Assumption 2. The target spacecraft is out of control with no external disturbances (i.e. $\boldsymbol{\tau}_t$ and $\boldsymbol{d}_t$ in Eq.(14) equal zero), and is tumbling freely in space. The external disturbance $\boldsymbol{d}_L$, and the uncertain stuck fault $\bar{\boldsymbol{F}}_C$ in Eq.(22) are unknown but bounded. Thus, there always exists positive but unknown constants d_{dist} and $\bar{F}_{stk}$ such that

$$\left\|\boldsymbol{d}_L\right\| \le d_{dist},\ \left\|\bar{\boldsymbol{F}}_C\right\| \le \bar{F}_{stk} \text{ and } \left\|\boldsymbol{R}_{Lc}\boldsymbol{D}\boldsymbol{E}\bar{\boldsymbol{F}}_C\right\| + \left\|\boldsymbol{d}_L\right\| \le d_{dist} + \left\|\boldsymbol{D}\right\|\bar{F}_{stk} \triangleq d \tag{23}$$

where the notation $\|\bullet\|$ denote the Euclidean norm of vectors and the induced norm for matrices.

Assumption 3. The matrix $\boldsymbol{D}(\boldsymbol{I}-\boldsymbol{E})$ is full-row rank, which implicitly means that the remaining active thrusters are able to produce a sufficient force for the chaser to perform the rendezvous mission. The thruster pairs can only partially lose its effectiveness, i.e., $E_i \in [0,1)$, and the faulty thrusters are still controllable.

The existence of Assumption 3 is to satisfy the fault compensability properties [50], then it is possible to design a passive fault-tolerant controller to insure the considered fault can be fully compensable.

Remark 4. The docking axis of the chaser spacecraft should track the target as the two spacecraft move. However, this paper studies the relative position at the rendezvous phase and the design of the attitude controller is outside the scope of this work. The attitude controllers for rendezvous and docking with a tumbling target spacecraft have been presented in the references such as [19-20] and so on.

5.1 Fixed-time Controller Design with no External Disturbance or Thruster Faults

For this case, because the thruster faults and external disturbance are not taken into account, the LOS based equation of relative motion (22) can be simplified to

$$\boldsymbol{A}_2\ddot{\boldsymbol{x}} + \boldsymbol{B}_2 = \boldsymbol{R}_{Lc}\boldsymbol{D}\boldsymbol{F}_{\boldsymbol{C1}} \tag{24}$$

Then, following statements can be made.

Theorem 2. For the LOS based equation of relative motion given by Eq.(24) under the Assumptions 1 and 2, if the fixed-time SM is chosen as Eq.(18) and the fixed-time controller is chosen as

$$\begin{aligned}\boldsymbol{F}_{\boldsymbol{C1}} = &-\boldsymbol{D}^{+}\boldsymbol{R}_{Lc}^{-1}\boldsymbol{A}_2\left[\boldsymbol{\alpha}_2 sig(\boldsymbol{S})^{p_2} + \boldsymbol{\beta}_2 sig(\boldsymbol{S})^{g_2}\right] + \boldsymbol{D}^{+}\boldsymbol{R}_{Lc}^{-1}\boldsymbol{B}_2 \\ &- \boldsymbol{D}^{+}\boldsymbol{R}_{Lc}^{-1}\boldsymbol{A}_2\mathrm{diag}\left(\left|\boldsymbol{\alpha}_1 sig(\boldsymbol{x})^{p_1} + \boldsymbol{\beta}_1 sig(\boldsymbol{x})^{g_1}\right|^{k_1-1}\right)\left[\boldsymbol{\alpha}_1\mathrm{diag}\left(|\boldsymbol{x}|^{p_1-1}\right)\dot{\boldsymbol{x}} + \boldsymbol{\beta}_1\mathrm{diag}\left(|\boldsymbol{x}|^{g_1-1}\right)\dot{\boldsymbol{x}}\right]\end{aligned} \tag{25}$$

where $\boldsymbol{\alpha}_2, \boldsymbol{\beta}_2, p_2, g_2$ are the controller parameters and satisfy $\boldsymbol{\alpha}_2 \in \mathrm{diag}(\alpha_{2i})$, $\boldsymbol{\beta}_2 \in \mathrm{diag}(\beta_{2i})$, $\alpha_{2i} > 0$, $\beta_{2i} > 0$, for $i = 1,2,3$, $p_2 \in (0,1)$, and $g_2 > 1$. $\boldsymbol{D}^{+} = \boldsymbol{D}^{\mathrm{T}}\left(\boldsymbol{D}\boldsymbol{D}^{\mathrm{T}}\right)^{-1}$ denotes the pseudo-inverse of $\boldsymbol{D}$ and $\boldsymbol{D}$ should satisfy full-row rank. Then the states of the system converge to origin in a fixed-time T, whose bound is independent of the initial values of system states and can be conservatively estimated as

$$T \le T_x + T_{S1} \le \frac{1}{\lambda_{\min}(\boldsymbol{\alpha}_2)^{k_1}(1-p_1k_1)} + \frac{1}{\lambda_{\min}(\boldsymbol{\beta}_2)^{k_1}(g_1k_1-1)} + \frac{1}{\lambda_{\min}(\boldsymbol{\alpha}_2)(1-p_2)} + \frac{1}{2^{1-g_2}\lambda_{\min}(\boldsymbol{\beta}_2)(g_2-1)} \tag{26}$$

Proof: The candidate Lyapunov function is defined as $V_{S1} = \boldsymbol{S}^{\mathrm{T}}\boldsymbol{S}$. Taking the derivative of the fixed-time SM, Eq.(18), yields

$$\dot{\boldsymbol{S}} = \ddot{\boldsymbol{x}} + \mathrm{diag}\left(\left|\boldsymbol{\alpha}_1 sig(\boldsymbol{x})^{p_1} + \boldsymbol{\beta}_1 sig(\boldsymbol{x})^{g_1}\right|^{k_1-1}\right)\left[\boldsymbol{\alpha}_1\mathrm{diag}\left(|\boldsymbol{x}|^{p_1-1}\right)\dot{\boldsymbol{x}} + \boldsymbol{\beta}_1\mathrm{diag}\left(|\boldsymbol{x}|^{g_1-1}\right)\dot{\boldsymbol{x}}\right] \tag{27}$$

Taking the derivative of V_{S1} and substituting for $\dot{\boldsymbol{S}}$, one has

$$\begin{aligned}\dot{V}_{S1} &= 2\boldsymbol{S}^{\mathrm{T}}\dot{\boldsymbol{S}} = 2\boldsymbol{S}^{\mathrm{T}}\left\{\ddot{\boldsymbol{x}} + \mathrm{diag}\left(\left|\boldsymbol{\alpha}_1 sig(\boldsymbol{x})^{p_1} + \boldsymbol{\beta}_1 sig(\boldsymbol{x})^{g_1}\right|^{k_1-1}\right)\left[\boldsymbol{\alpha}_1\mathrm{diag}\left(|\boldsymbol{x}|^{p_1-1}\right)\dot{\boldsymbol{x}} + \boldsymbol{\beta}_1\mathrm{diag}\left(|\boldsymbol{x}|^{g_1-1}\right)\dot{\boldsymbol{x}}\right]\right\} \\ &= 2\boldsymbol{S}^{\mathrm{T}}\left\{\boldsymbol{A}_2^{+}\boldsymbol{R}_{Lc}\boldsymbol{D}\boldsymbol{F}_{\boldsymbol{C1}} - \boldsymbol{A}_2^{+}\boldsymbol{B}_2 + \mathrm{diag}\left(\left|\boldsymbol{\alpha}_1 sig(\boldsymbol{x})^{p_1} + \boldsymbol{\beta}_1 sig(\boldsymbol{x})^{g_1}\right|^{k_1-1}\right)\left[\boldsymbol{\alpha}_1\mathrm{diag}\left(|\boldsymbol{x}|^{p_1-1}\right)\dot{\boldsymbol{x}} + \boldsymbol{\beta}_1\mathrm{diag}\left(|\boldsymbol{x}|^{g_1-1}\right)\dot{\boldsymbol{x}}\right]\right\} \\ &= 2\boldsymbol{S}^{\mathrm{T}}\left[-\boldsymbol{\alpha}_2 sig(\boldsymbol{S})^{p_2} - \boldsymbol{\beta}_2 sig(\boldsymbol{S})^{g_2}\right] \\ &\le -2\lambda_{\min}(\boldsymbol{\alpha}_2)\left[\left(S_1^2\right)^{\frac{1+p_2}{2}} + \left(S_2^2\right)^{\frac{1+p_2}{2}} + \left(S_3^2\right)^{\frac{1+p_2}{2}}\right] - 2\lambda_{\min}(\boldsymbol{\beta}_2)\left[\left(S_1^2\right)^{\frac{1+g_2}{2}} + \left(S_2^2\right)^{\frac{1+g_2}{2}} + \left(S_3^2\right)^{\frac{1+g_2}{2}}\right]\end{aligned} \tag{28}$$

Using Lemma 5 and Proposition 2 gives

$$\dot{V}_{S1} \le -2\lambda_{\min}(\boldsymbol{\alpha_2})\left(\boldsymbol{S}^{\mathrm{T}}\boldsymbol{S}\right)^{\frac{1+p_2}{2}} - 2^{2-g_2}\lambda_{\min}(\boldsymbol{\beta_2})\left(\boldsymbol{S}^{\mathrm{T}}\boldsymbol{S}\right)^{\frac{1+g_2}{2}} = -2\lambda_{\min}(\boldsymbol{\alpha_2})V_{S1}^{\frac{1+p_2}{2}} - 2^{2-g_2}\lambda_{\min}(\boldsymbol{\beta_2})V_{S1}^{\frac{1+g_2}{2}} \tag{29}$$

From Lemma 1, the origin of the system in Eq.(24) is fixed-time stable, and all of the states arrive at the fixed-time SM, Eq.(18), in a fixed-time T_{S1}, which satisfies

$$T_{S1} \le \frac{1}{\lambda_{\min}(\boldsymbol{\alpha_2})(1-p_2)} + \frac{1}{2^{1-g_2}\lambda_{\min}(\boldsymbol{\beta_2})(g_2-1)}. \tag{30}$$

Combining Eq.(30) and Eq.(19), the complete convergence time of rendezvous and docking can be expressed as

$T \le T_x + T_{S1} \le \frac{1}{\lambda_{\min}(\boldsymbol{\alpha}_1)^{k_1}(1-p_1k_1)} + \frac{1}{\lambda_{\min}(\boldsymbol{\beta}_1)^{k_1}(g_1k_1-1)} + \frac{1}{\lambda_{\min}(\boldsymbol{\alpha}_2)(1-p_2)} + \frac{1}{2^{1-g_2}\lambda_{\min}(\boldsymbol{\beta}_2)(g_2-1)}$. Thus, the bound of the convergence time T can be conservatively estimated, even if we have no knowledge of the initial and instantaneous values of the system states. Hence, the proof of Theorem 2 is completed.

5.2 Adaptive Fixed-time Controller Design with External Disturbance and Thruster Faults

The controller in Eq.(25) is designed based on the assumption that there is no external disturbance and no fault or failure of the spacecraft system components will ever occur. However, this assumption is rarely satisfied in practice because the disturbance is unavoidable and some catastrophic faults may occur due to malfunctions, especially in the thrusters. In this section, we will use the dynamic model in Eq.(22) and investigate the fixed-time rendezvous and docking problem with external disturbance and thruster faults. To solve this problem, an adaptive fixed-time finite controller is designed to guarantee the fixed-time SM converges to the residual set $\boldsymbol{S}=0$ in fixed time sense.

Theorem 3. Consider the LOS based equation of relative motion in Eq.(14) for rendezvous and docking with thruster faults and external disturbance under Assumption 1 to 3. The adaptive fixed-time based controller is chosen as

$$\begin{aligned}\boldsymbol{F_C} = &-\left[\boldsymbol{D}\left(\boldsymbol{I}-\hat{\boldsymbol{E}}\right)\right]^{+}\boldsymbol{R}_{Lc}^{-1}\boldsymbol{A}_2\left[\boldsymbol{\alpha}_3 sig\left(\boldsymbol{S}\right)^{p_3}+\boldsymbol{\beta}_3 sig\left(\boldsymbol{S}\right)^{g_3}\right]+\left[\boldsymbol{D}\left(\boldsymbol{I}-\hat{\boldsymbol{E}}\right)\right]^{+}\boldsymbol{R}_{Lc}^{-1}\boldsymbol{B}_2\\ &-\left[\boldsymbol{D}\left(\boldsymbol{I}-\hat{\boldsymbol{E}}\right)\right]^{+}\boldsymbol{R}_{Lc}^{-1}\boldsymbol{A}_2\mathrm{diag}\left(\left|\boldsymbol{\alpha}_1 sig(\boldsymbol{x})^{p_1}+\boldsymbol{\beta}_1 sig(\boldsymbol{x})^{g_1}\right|^{k_1-1}\right)\\ &\left[\boldsymbol{\alpha}_1\mathrm{diag}\left(\left|\boldsymbol{x}\right|^{p_1-1}\right)\dot{\boldsymbol{x}}+\boldsymbol{\beta}_1\mathrm{diag}\left(\left|\boldsymbol{x}\right|^{g_1-1}\right)\dot{\boldsymbol{x}}\right]-\left[\boldsymbol{D}\left(\boldsymbol{I}-\hat{\boldsymbol{E}}\right)\right]^{+}\boldsymbol{R}_{Lc}^{-1}\hat{d}\frac{\boldsymbol{S}}{\|\boldsymbol{S}\|}\end{aligned} \tag{31}$$

and updated by

$$\dot{\hat{d}} = \frac{1}{\theta_0 c_1}\|\boldsymbol{S}\|\left\|\boldsymbol{A}_2^{+}\right\| - \frac{\sigma_1}{2\theta_0 c_1}\hat{d} \tag{32}$$

$$\dot{\hat{\boldsymbol{\Theta}}} = \frac{1}{\theta_0 c_2} diag\left(\boldsymbol{F_C}\right)^{\mathrm{T}}\boldsymbol{D}^{\mathrm{T}}\boldsymbol{R}_{Lc}^{\mathrm{T}}\boldsymbol{S} - \frac{\sigma_2}{2\theta_0 c_2}\hat{\boldsymbol{\Theta}} \tag{33}$$

where the gains c_1, c_2 and θ_0 satisfy the constraints

$$c_1 = \frac{\sigma_1\left(2\theta_1-1\right)}{2\theta_1} \qquad c_2 = \frac{\sigma_2\left(2\theta_2-1\right)}{2\theta_2} \qquad \theta_0^{\frac{p_2+1}{2}}+\theta_0-1=0 \qquad \theta_0\in(0,1) \tag{34}$$

where $\sigma_1,\sigma_2,\boldsymbol{\alpha}_3,\boldsymbol{\beta}_3,\theta_1,\theta_2,p_3,g_3$ are the controller parameters and satisfy $\sigma_1,\sigma_2>0$, $p_3\in(0,1)$, $g_3>1$, $\theta_1>\frac{1}{2}$, $\theta_2>\frac{1}{2}$, $\boldsymbol{\alpha}_3\in\mathrm{diag}\left(\alpha_{3i}\right)$, $\boldsymbol{\beta}_3\in\mathrm{diag}\left(\beta_{3i}\right)$, $\alpha_{3i}>0$, $\beta_{3i}>0$, for $i=1,2,3$. The adaptive terms $\hat{d}$ and $\hat{\boldsymbol{\Theta}}$ are estimates of the unknown parameters d and $\boldsymbol{\Theta}$, and $\hat{\boldsymbol{\Theta}}$ satisfies $\hat{\boldsymbol{E}}\boldsymbol{F_C}=\mathrm{diag}\left(\boldsymbol{F_C}\right)\hat{\boldsymbol{\Theta}}$. Then the estimation errors $\tilde{d}=d-\hat{d}$ and $\tilde{\boldsymbol{\Theta}}=\boldsymbol{\Theta}-\hat{\boldsymbol{\Theta}}$ converge to a residual set. Moreover, we assume that there exists an unknown constant Δ and a compact set D_1 such that

$$D_1 = \left\{\left(\tilde{d},\tilde{\boldsymbol{\Theta}}\right)\middle|\ \tilde{d}\le\Delta,\tilde{\boldsymbol{\Theta}}^{\mathrm{T}}\tilde{\boldsymbol{\Theta}}\le\Delta\right\} \tag{35}$$

Then the trajectory of the closed-loop system will converge to the region D_2 in a fixed time T_{S2}, where the region D_2 and the convergence time T_{S2} are given by

$$D_2 = \left\{\lim_{t\to T_{S2}}\boldsymbol{S}(t)\middle| V_S\le\min\left\{\left(\frac{\vartheta}{\eta_1(1-\theta)}\right)^{\frac{2}{p_3+1}},\left(\frac{2^{g_3-1}\vartheta}{\eta_2(1-\theta)}\right)^{\frac{2}{g_3+1}}\right\}\right\} \tag{36}$$

$$T_{S2}\le\frac{1}{\eta_1\theta(1-p_3)}+\frac{2^{g_3-1}}{\eta_2\theta(g_3-1)} \tag{37}$$

without any knowledge of the initial or instantaneous values of the system states, and where

$$\vartheta = \begin{cases}\vartheta_1 & if\ :\Delta\le\min\left\{\frac{1}{\sqrt{\theta_0 c_1}},\frac{1}{\sqrt{\theta_0 c_2}}\right\}\\ \vartheta_1+2\left(\theta_0 c_{\max}\Delta^2\right)^{\frac{g_3+1}{2}}-2\left(\theta_0 c_{\max}\Delta^2\right) & if\ :\Delta\ge\min\left\{\frac{1}{\sqrt{\theta_0 c_1}},\frac{1}{\sqrt{\theta_0 c_2}}\right\}\end{cases},\quad c_{\max}=\max\left\{c_1,c_2,c_3\right\},\ \text{and}$$

$$\vartheta_1 = \frac{\theta_1\sigma_1}{2}d^2 + \frac{\theta_1\sigma_2}{2}\boldsymbol{\Theta}^{\mathrm{T}}\boldsymbol{\Theta} + 2\theta_0^{\frac{p_3+1}{2}}\vartheta_0 .$$

Proof: Consider the candidate Lyapunov function V_{S2} given by

$$V_{S2} = \boldsymbol{S}^{\mathrm{T}}\boldsymbol{S} + \theta_0 c_1\tilde{d}^2 + \theta_0 c_2\tilde{\boldsymbol{\Theta}}^{\mathrm{T}}\tilde{\boldsymbol{\Theta}} \tag{38}$$

where $\tilde{d} = d - \hat{d}$ and $\tilde{\boldsymbol{\Theta}} = \boldsymbol{\Theta} - \hat{\boldsymbol{\Theta}}$. Taking the derivative of this Lyapunov function we have

$$\begin{aligned}
\dot{V}_{S2} &= 2\boldsymbol{S}^{\mathrm{T}}\dot{\boldsymbol{S}} + 2\theta_0 c_1\tilde{d}\dot{\tilde{d}} + 2\theta_0 c_2\tilde{\boldsymbol{\Theta}}^{\mathrm{T}}\dot{\tilde{\boldsymbol{\Theta}}} \\
&= 2\boldsymbol{S}^{\mathrm{T}}\left\{\ddot{\boldsymbol{x}} + \mathrm{diag}\left(\left|\boldsymbol{\alpha}_1 sig(\boldsymbol{x})^{p_1} + \boldsymbol{\beta}_1 sig(\boldsymbol{x})^{g_1}\right|^{k_1-1}\right)\left[\boldsymbol{\alpha}_1\mathrm{diag}\left(|\boldsymbol{x}|^{p_1-1}\right)\dot{\boldsymbol{x}} + \boldsymbol{\beta}_1\mathrm{diag}\left(|\boldsymbol{x}|^{g_1-1}\right)\dot{\boldsymbol{x}}\right]\right\} + 2\theta_0 c_1\tilde{d}\dot{\tilde{d}} + 2\theta_0 c_2\tilde{\boldsymbol{\Theta}}^{\mathrm{T}}\dot{\tilde{\boldsymbol{\Theta}}} \\
&= 2\boldsymbol{S}^{\mathrm{T}}\left\{-\boldsymbol{A}_2^{+}\boldsymbol{B}_2 + \boldsymbol{A}_2^{+}\boldsymbol{R}_{Lc}\boldsymbol{D}\left(\boldsymbol{I}-\boldsymbol{E}\right)\boldsymbol{F}_C + \boldsymbol{A}_2^{+}\left(\boldsymbol{d} + \boldsymbol{DE}\bar{\boldsymbol{F}}\right)\right. \\
&\quad \left. + \mathrm{diag}\left(\left|\boldsymbol{\alpha}_1 sig(\boldsymbol{x})^{p_1} + \boldsymbol{\beta}_1 sig(\boldsymbol{x})^{g_1}\right|^{k_1-1}\right)\left[\boldsymbol{\alpha}_1\mathrm{diag}\left(|\boldsymbol{x}|^{p_1-1}\right)\dot{\boldsymbol{x}} + \boldsymbol{\beta}_1\mathrm{diag}\left(|\boldsymbol{x}|^{g_1-1}\right)\dot{\boldsymbol{x}}\right]\right\} + 2\theta_0 c_1\tilde{d}\dot{\tilde{d}} + 2\theta_0 c_2\tilde{\boldsymbol{\Theta}}^{\mathrm{T}}\dot{\tilde{\boldsymbol{\Theta}}}
\end{aligned} \tag{39}$$

Define the estimation error of the fault value as $\tilde{\boldsymbol{E}} = \boldsymbol{E} - \hat{\boldsymbol{E}}$. Substituting this error into Eq.(39) yields

$$\begin{aligned}
\dot{V}_{S2} &= 2\boldsymbol{S}^{\mathrm{T}}\left\{-\boldsymbol{A}_2^{+}\boldsymbol{B}_2 + \boldsymbol{A}_2^{+}\boldsymbol{R}_{Ls}\boldsymbol{D}\left(\boldsymbol{I}-\hat{\boldsymbol{E}}\right)\boldsymbol{F}_C - \boldsymbol{A}_2^{+}\boldsymbol{R}_{Lc}\boldsymbol{D}\tilde{\boldsymbol{E}}\boldsymbol{F}_C + \boldsymbol{A}_2^{+}\left(\boldsymbol{d} + \boldsymbol{DE}\bar{\boldsymbol{F}}_C\right)\right. \\
&\quad \left. + \mathrm{diag}\left(\left|\boldsymbol{\alpha}_1 sig(\boldsymbol{x})^{p_1} + \boldsymbol{\beta}_1 sig(\boldsymbol{x})^{g_1}\right|^{k_1-1}\right)\left[\boldsymbol{\alpha}_1\mathrm{diag}\left(|\boldsymbol{x}|^{p_1-1}\right)\dot{\boldsymbol{x}} + \boldsymbol{\beta}_1\mathrm{diag}\left(|\boldsymbol{x}|^{g_1-1}\right)\dot{\boldsymbol{x}}\right]\right\} + 2\theta_0 c_1\tilde{d}\dot{\tilde{d}} + 2\theta_0 c_2\tilde{\boldsymbol{\Theta}}^{\mathrm{T}}\dot{\tilde{\boldsymbol{\Theta}}}
\end{aligned} \tag{40}$$

Substituting the adaptive fixed-time controller, Eq.(31), into Eq.(40) gives

$$\begin{aligned}
\dot{V}_{S2} &= 2\boldsymbol{S}^{\mathrm{T}}\left[-\boldsymbol{\alpha}_3 sig\left(\boldsymbol{S}\right)^{p_3} - \boldsymbol{\beta}_3 sig\left(\boldsymbol{S}\right)^{g_3} - \boldsymbol{A}_2^{+}\hat{d}\frac{\boldsymbol{S}}{\|\boldsymbol{S}\|} - \boldsymbol{A}_2^{+}\boldsymbol{R}_{Lc}\boldsymbol{D}\tilde{\boldsymbol{E}}\boldsymbol{F}_C + \boldsymbol{A}_2^{+}\left(\boldsymbol{d} + \boldsymbol{DE}\bar{\boldsymbol{F}}_C\right)\right] + 2\theta_0 c_1\tilde{d}\dot{\tilde{d}} + 2\theta_0 c_2\tilde{\boldsymbol{\Theta}}^{\mathrm{T}}\dot{\tilde{\boldsymbol{\Theta}}} \\
&\le -2\lambda_{\min}\left(\boldsymbol{\alpha}_3\right)\left(\boldsymbol{S}^{\mathrm{T}}\boldsymbol{S}\right)^{\frac{1+p_3}{2}} - 2^{2-g_3}\lambda_{\min}\left(\boldsymbol{\beta}_3\right)\left(\boldsymbol{S}^{\mathrm{T}}\boldsymbol{S}\right)^{\frac{1+g_3}{2}} - 2\|\boldsymbol{S}\|\left\|\boldsymbol{A}_2^{+}\right\|\hat{d} - 2\boldsymbol{S}^{\mathrm{T}}\boldsymbol{A}_2^{+}\boldsymbol{R}_{Lc}\boldsymbol{D}diag\left(\boldsymbol{F}_C\right)\tilde{\Theta} \\
&\quad + 2\|\boldsymbol{S}\|\left\|\boldsymbol{A}_2^{+}\right\|d + 2\theta_0 c_1\tilde{d}\dot{\tilde{d}} + 2\theta_0 c_2\tilde{\boldsymbol{\Theta}}^{\mathrm{T}}\dot{\tilde{\boldsymbol{\Theta}}} \\
&\le -2\lambda_{\min}\left(\boldsymbol{\alpha}_3\right)\left(\boldsymbol{S}^{\mathrm{T}}\boldsymbol{S}\right)^{\frac{1+p_3}{2}} - 2^{2-g_3}\lambda_{\min}\left(\boldsymbol{\beta}_3\right)\left(\boldsymbol{S}^{\mathrm{T}}\boldsymbol{S}\right)^{\frac{1+g_3}{2}} + 2\|\boldsymbol{S}\|\left\|\boldsymbol{A}_2^{+}\right\|\tilde{d} \\
&\quad - 2\boldsymbol{S}^{\mathrm{T}}\boldsymbol{A}_2^{+}\boldsymbol{R}_{Lc}\boldsymbol{D}diag\left(\boldsymbol{F}_C\right)\tilde{\Theta} - 2\theta_0 c_1\tilde{d}\dot{\tilde{d}} - 2\theta_0 c_2\tilde{\boldsymbol{\Theta}}^{\mathrm{T}}\dot{\tilde{\boldsymbol{\Theta}}}
\end{aligned} \tag{41}$$

Using the adaptive laws in Eq.(32) and Eq.(33), we have

$$\dot{V}_{S2} \le -2\lambda_{\min}\left(\boldsymbol{\alpha}_3\right)\left(\boldsymbol{S}^{\mathrm{T}}\boldsymbol{S}\right)^{\frac{1+p_3}{2}} - 2^{2-g_3}\lambda_{\min}\left(\boldsymbol{\beta}_3\right)\left(\boldsymbol{S}^{\mathrm{T}}\boldsymbol{S}\right)^{\frac{1+g_3}{2}} + \sigma_1\tilde{d}\hat{d} + \sigma_2\tilde{\boldsymbol{\Theta}}^{\mathrm{T}}\hat{\boldsymbol{\Theta}} \tag{42}$$

For any $\theta_1 > \frac{1}{2}$ and $\theta_2 > \frac{1}{2}$, one has

$$\sigma_1\tilde{d}\hat{d} = -\sigma_1\tilde{d}\left(\tilde{d} - d\right) \le \sigma_1\left(-\frac{2\theta_1 - 1}{2\theta_1}\tilde{d}^2 + \frac{\theta_1}{2}d^2\right) = -c_1\tilde{d}^2 + \frac{\theta_1\sigma_1}{2}d^2 \tag{43}$$

$$\sigma_2\tilde{\boldsymbol{\Theta}}^{\mathrm{T}}\hat{\boldsymbol{\Theta}} = \sigma_2\tilde{\boldsymbol{\Theta}}\left(\tilde{\boldsymbol{\Theta}} - \boldsymbol{\Theta}\right) \le \sigma_2\left(-\frac{2\theta_1 - 1}{2\theta_1}\tilde{\boldsymbol{\Theta}}^{\mathrm{T}}\tilde{\boldsymbol{\Theta}} + \frac{\theta_1}{2}\boldsymbol{\Theta}^{\mathrm{T}}\boldsymbol{\Theta}\right) = -c_1\tilde{\boldsymbol{\Theta}}^{\mathrm{T}}\tilde{\boldsymbol{\Theta}} + \frac{\theta_1\sigma_2}{2}\boldsymbol{\Theta}^{\mathrm{T}}\boldsymbol{\Theta} \tag{44}$$

Then, further simplification of Eq.(42) gives

$$
\begin{aligned}
\dot{V}_{S2} \le & -2\lambda_{\min}(\boldsymbol{\alpha}_3)\left(\boldsymbol{S}^{\mathrm{T}}\boldsymbol{S}\right)^{\frac{1+p_3}{2}} - \left(\theta_0 c_1 \tilde{d}^2\right)^{\frac{1+p_3}{2}} - \left(\theta_0 c_2 \tilde{\boldsymbol{\Theta}}^{\mathrm{T}}\tilde{\boldsymbol{\Theta}}\right)^{\frac{1+p_3}{2}} \\
& - 2^{2-g_3}\lambda_{\min}(\boldsymbol{\beta}_3)\left(\boldsymbol{S}^{\mathrm{T}}\boldsymbol{S}\right)^{\frac{1+g_3}{2}} - \left(\theta_0 c_1 \tilde{d}^2\right)^{\frac{1+g_3}{2}} - \left(\theta_0 c_2 \tilde{\boldsymbol{\Theta}}^{\mathrm{T}}\tilde{\boldsymbol{\Theta}}\right)^{\frac{1+g_3}{2}} \\
& + \left(\theta_0 c_1 \tilde{d}^2\right)^{\frac{1+p_3}{2}} + \left(\theta_0 c_2 \tilde{\boldsymbol{\Theta}}^{\mathrm{T}}\tilde{\boldsymbol{\Theta}}\right)^{\frac{1+p_3}{2}} + \left(\theta_0 c_1 \tilde{d}^2\right)^{\frac{1+g_3}{2}} + \left(\theta_0 c_2 \tilde{\boldsymbol{\Theta}}^{\mathrm{T}}\tilde{\boldsymbol{\Theta}}\right)^{\frac{1+g_3}{2}} \\
& - \theta_0^{\frac{1+p_3}{2}} c_1 \tilde{d}^2 - \theta_0^{\frac{1+p_3}{2}} c_2 \tilde{\boldsymbol{\Theta}}^{\mathrm{T}}\tilde{\boldsymbol{\Theta}} - \left(1-\theta_0^{\frac{1+p_3}{2}}\right) c_1 \tilde{d}^2 - \left(1-\theta_0^{\frac{1+p_3}{2}}\right) c_2 \tilde{\boldsymbol{\Theta}}^{\mathrm{T}}\tilde{\boldsymbol{\Theta}} + \frac{\theta_1\sigma_1}{2} d^2 + \frac{\theta_1\sigma_2}{2}\boldsymbol{\Theta}^{\mathrm{T}}\boldsymbol{\Theta}
\end{aligned} \tag{45}
$$

Case 1: If $c_1\tilde{d}^2 \ge 1$, one has

$$
\left(c_1\tilde{d}^2\right)^{\frac{p_3+1}{2}} - c_1\tilde{d}^2 < 0 \tag{46}
$$

Case 2: If $c_1\tilde{d}^2 < 1$, then using the basic properties of powers,

$$
0 < \left(c_1\tilde{d}^2\right)^{\frac{p_3+1}{2}} - c_1\tilde{d}^2 < \vartheta_0 \tag{47}
$$

where $\vartheta_0 = p_0^{p_0/(1-p_0)} - p_0^{1/(1-p_0)} > 0$ and $p_0 = (p_3+1)/2$

Combining Eqs. (46) and (47) leads to

$$
\left(c_1\tilde{d}^2\right)^{\frac{p_3+1}{2}} - c_1\tilde{d}^2 < \vartheta_0 \tag{48}
$$

Similarly, we can obtain the following inequality

$$
\left(c_2\tilde{\boldsymbol{\Theta}}^{\mathrm{T}}\tilde{\boldsymbol{\Theta}}\right)^{\frac{p_3+1}{2}} - c_2\tilde{\boldsymbol{\Theta}}^{\mathrm{T}}\tilde{\boldsymbol{\Theta}} < \vartheta_0 \tag{49}
$$

Note that $1-\theta_0^{\frac{p_2+1}{2}} = \theta_0$ and define $\eta_1 = \min\left\{2\lambda_{\min}(\boldsymbol{\alpha}_3), 1\right\}$, $\eta_2 = \min\left\{2^{2-g_3}\lambda_{\min}(\boldsymbol{\beta}_3), 1\right\}$. Then Eq.(45) can be written as

$$
\begin{aligned}
\dot{V}_{S2} \le & -\eta_1\left[\left(\boldsymbol{S}^{\mathrm{T}}\boldsymbol{S}\right)^{\frac{1+p_3}{2}} + \left(\theta_0 c_1 \tilde{d}^2\right)^{\frac{1+p_3}{2}} + \left(\theta_0 c_2 \tilde{\boldsymbol{\Theta}}^{\mathrm{T}}\tilde{\boldsymbol{\Theta}}\right)^{\frac{1+p_3}{2}}\right] \\
& - \eta_2\left[\left(\boldsymbol{S}^{\mathrm{T}}\boldsymbol{S}\right)^{\frac{1+g_3}{2}} + \left(\theta_0 c_1 \tilde{d}^2\right)^{\frac{1+g_3}{2}} + \left(\theta_0 c_2 \tilde{\boldsymbol{\Theta}}^{\mathrm{T}}\tilde{\boldsymbol{\Theta}}\right)^{\frac{1+g_3}{2}}\right] \\
& + \left(\theta_0 c_1 \tilde{d}^2\right)^{\frac{1+g_3}{2}} + \left(\theta_0 c_2 \tilde{\boldsymbol{\Theta}}^{\mathrm{T}}\tilde{\boldsymbol{\Theta}}\right)^{\frac{1+g_3}{2}} - \left(1-\theta_0^{\frac{1+p_3}{2}}\right) c_1 \tilde{d}^2 - \left(1-\theta_0^{\frac{1+p_3}{2}}\right) c_2 \tilde{\boldsymbol{\Theta}}^{\mathrm{T}}\tilde{\boldsymbol{\Theta}} \\
& + \frac{\theta_1\sigma_1}{2} d^2 + \frac{\theta_1\sigma_2}{2}\boldsymbol{\Theta}^{\mathrm{T}}\boldsymbol{\Theta} + 2\theta_0^{\frac{p_2+1}{2}}\vartheta_0 \\
\le & -\eta_1 V_{S2}^{(p_3+1)/2} - 2^{1-g_3}\eta_2 V_{S2}^{(g_3+1)/2} + \vartheta_1 \\
& + \left(\theta_0 c_1 \tilde{d}^2\right)^{\frac{1+g_3}{2}} + \left(\theta_0 c_2 \tilde{\boldsymbol{\Theta}}^{\mathrm{T}}\tilde{\boldsymbol{\Theta}}\right)^{\frac{1+g_3}{2}} - \theta_0 c_1 \tilde{d}^2 - \theta_0 c_2 \tilde{\boldsymbol{\Theta}}^{\mathrm{T}}\tilde{\boldsymbol{\Theta}}
\end{aligned} \tag{50}
$$

where Proposition 2 has been used and $\vartheta_1 = \frac{\theta_1\sigma_1}{2} d^2 + \frac{\theta_1\sigma_2}{2}\boldsymbol{\Theta}^{\mathrm{T}}\boldsymbol{\Theta} + 2\theta_0^{\frac{p_3+1}{2}}\vartheta_0$.

In addition, if Eq.(35) holds, the following two cases are considered:

Case 1: If $\Delta \le \min\left\{\frac{1}{\sqrt{\theta_0 c_1}}, \frac{1}{\sqrt{\theta_0 c_2}}\right\}$, one has

$$\left(\theta_0 c_1 \tilde{d}^2\right)^{\frac{g_3+1}{2}} \le \theta_0 c_1 \tilde{d}^2,\ \left(\theta_0 c_2 \tilde{\boldsymbol{\Theta}}^{\mathrm{T}} \tilde{\boldsymbol{\Theta}}\right)^{\frac{g_3+1}{2}} \le \theta_0 c_2 \tilde{\boldsymbol{\Theta}}^{\mathrm{T}} \tilde{\boldsymbol{\Theta}}, \tag{51}$$

Then, Eq.(50) can be simplified to give

$$\dot{V}_{S2} \le -\eta_1 V_{S2}^{(p_3+1)/2} - 2^{1-g_3} \eta_2 V_{S2}^{(g_3+1)/2} + \vartheta_1 \tag{52}$$

Case 2: If $\Delta \ge \min\left\{\frac{1}{\sqrt{\theta_0 c_1}}, \frac{1}{\sqrt{\theta_0 c_2}}\right\}$, we have

$$\left(\theta_0 c_1 \tilde{d}^2\right)^{\frac{g_3+1}{2}} + \left(\theta_0 c_2 \tilde{\boldsymbol{\Theta}}^{\mathrm{T}} \tilde{\boldsymbol{\Theta}}\right)^{\frac{g_3+1}{2}} - \theta_0 c_1 \tilde{d}^2 - \theta_0 c_2 \tilde{\boldsymbol{\Theta}}^{\mathrm{T}} \tilde{\boldsymbol{\Theta}} \le 2\left(\theta_0 c_{\max} \Delta^2\right)^{\frac{g_3+1}{2}} - 2\left(\theta_0 c_{\max} \Delta^2\right) \tag{53}$$

where $c_{\max} = \max\{c_1, c_2\}$.

Then, Eq.(50) can be rewritten as

$$\dot{V}_{S2} \le -\eta_1 V_{S2}^{(p_3+1)/2} - 2^{1-g_3} \eta_2 V_{S2}^{(g_3+1)/2} + \vartheta_1 + 2\left(\theta_0 c_{\max} \Delta^2\right)^{\frac{g_3+1}{2}} - 2\left(\theta_0 c_{\max} \Delta^2\right) \tag{54}$$

Combining Eqs. (52) and (54) leads to

$$\dot{V}_{S2} \le -\eta_1 V_{S2}^{(p_3+1)/2} - 2^{1-g_3} \eta_2 V_{S2}^{(g_3+1)/2} + \vartheta \tag{55}$$

where $\vartheta = \begin{cases} \vartheta_1 & if\ : \Delta \le \min\left\{\frac{1}{\sqrt{\theta_0 c_1}}, \frac{1}{\sqrt{\theta_0 c_2}}\right\} \\ \vartheta_1 + 2\left(\theta_0 c_{\max} \Delta^2\right)^{\frac{g_3+1}{2}} - 2\left(\theta_0 c_{\max} \Delta^2\right) & if\ : \Delta \ge \min\left\{\frac{1}{\sqrt{\theta_0 c_1}}, \frac{1}{\sqrt{\theta_0 c_2}}\right\} \end{cases}$

Then, using Proposition 1, the trajectory of the system in Eq.(55) is practical fixed-time stable. The residual set D_2 is calculated as

$$D_2 = \left\{ \lim_{t \to T_{S2}} \boldsymbol{S}(t) \middle| V_S \le \min\left\{ \left(\frac{\vartheta}{\eta_1 (1-\theta)}\right)^{\frac{2}{p_3+1}}, \left(\frac{2^{g_3-1} \vartheta}{\eta_2 (1-\theta)}\right)^{\frac{2}{g_3+1}} \right\} \right\} \tag{56}$$

and the settling time T_{S2} is given by

$$T_{S2} \le \frac{1}{\eta_1 \theta (1-p_3)} + \frac{2^{g_3-1}}{\eta_2 \theta (g_3-1)} \tag{57}$$

without any knowledge of the initial or instantaneous values of the system states. In addition, if the exact value of $V(\boldsymbol{x}_0)$ is known, the settling time T_{S2} is explicitly given by

$$T_{S2} \le \frac{2}{\eta_1 \theta (1-p_3)} \left| V_{S(0)} \right|^{(1-p_3)/2} \quad \overline{\mathrm{F}}\left(1, \frac{1-p_3}{g_3-p_3}, 1+\frac{1-p_3}{g_3-p_3}, -\frac{2^{1-g_3}\eta_2}{\eta_1} \left| V_{S2(0)} \right|^{(g_3-p_3)/2} \right) \tag{58}$$

where $\theta \in (0,1)$ and $V_{S2(0)}$ is the initial value of V_{S2}. Hence, the proof of Theorem 3 is completed.

Remark 5. Equation (45) can be rewritten as

$$\begin{aligned} \dot{V}_{S2} &\le -\mu \lambda_{\min}(\boldsymbol{\alpha}_3) \left(\boldsymbol{S}^T \boldsymbol{S} \right)^{\frac{p_3+1}{2}} - \left(\theta_0 c_1 \tilde{d}^2 \right)^{\frac{p_3+1}{2}} - \left(\theta_0 c_2 \tilde{\boldsymbol{\Theta}}^{\mathrm{T}} \tilde{\boldsymbol{\Theta}} \right)^{\frac{p_3+1}{2}} + \left(\theta_0 c_1 \tilde{d}^2 \right)^{\frac{p_3+1}{2}} + \left(\theta_0 c_2 \tilde{\boldsymbol{\Theta}}^{\mathrm{T}} \tilde{\boldsymbol{\Theta}} \right)^{\frac{p_3+1}{2}} \\ &\quad - \theta_0^{\frac{p_3+1}{2}} c_1 \tilde{d}^2 - \theta_0^{\frac{p_3+1}{2}} c_2 \tilde{\boldsymbol{\Theta}}^{\mathrm{T}} \tilde{\boldsymbol{\Theta}} + \frac{\sigma_1 \theta_1}{2} d^2 + \frac{\sigma_2 \theta_2}{2} \boldsymbol{\Theta}^{\mathrm{T}} \boldsymbol{\Theta} \\ &\le -\eta_1 V_{S2}^{(p_3+1)/2} + \vartheta_1 \end{aligned} \tag{59}$$

According to Lemma 3, the trajectory of this system is practical finite-time stable. Moreover, the fixed-time SM and estimation errors will converge to the residual set

$$D_3 = \left\{ \lim_{t \to T_{S3}} \left(\boldsymbol{S}, \tilde{d}, \tilde{\boldsymbol{\Theta}} \right) \middle| V_{S2} \le \left[\frac{\vartheta_1}{\eta_1 (1-\theta)} \right]^{\frac{2}{p_3+1}} \right\} \tag{60}$$

where T_{S3} is the time needed to reach the residual set and expressed as

$$T_{S3} \le \frac{2 V_{S2(0)}^{(1-p_3)/2}}{\eta_1 \theta (1-p_3)} \tag{61}$$

In conclusion, the estimation errors $\tilde{d}$ and $\tilde{\boldsymbol{\Theta}}$ will converge to the residual set D_3 in finite time T_{S3}. Thus, the assumption in Eq.(35) is reasonable

Remark 6. The above analysis shows that the parameters η_1, η_2 and ϑ are related to the band of attraction of the sliding surface. Hence, we can choose σ_1, σ_2 small enough and α_2, β_2 large enough to guarantee the motion along the sliding surface, i.e. $\boldsymbol{S} = 0$.

Remark 7. The preceding procedure for the selection of control parameters for the control strategy can summarized as follows:

1) Step 1: Set the homogeneity powers $p_i = g_i = k_1 = 1$, for $i = 1,2,3$, first. Then select suitable gain parameters $\boldsymbol{\alpha}_i, \boldsymbol{\beta}_i$, $i = 1,2,3$, which mainly affect the convergence time of control system.

2) Step 2: Select suitable homogeneity powers p_i, g_i, k_1, for $i = 1,2,3$, which mainly determine the

accuracy of control system.

3) Step 3: Select suitable gain parameters $\sigma_1, \sigma_2, \theta_1, \theta_2$, which mainly affect the fault tolerant capability, and robustness to external disturbances.

6. Simulation Results and Comparison

To verify the effectiveness of the proposed fixed-time sliding surface and controllers, the detailed simulations on a vehicle with six thruster pairs under various conditions are conducted using the model governed by Eq.(22) in conjunction with the proposed fixed-time controller in Eq.(25), and the adaptive fixed-time controller in Eq.(31). The numerical simulations are performed with MATLAB function 'ode4', and the fixed-step size is set as 0.1s. Each thruster pair contains two symmetric thrusters and the limited control force of each thruster is $F_{c\max,i} = 10$ N. The thruster configuration are illustrated in Fig.2, which cites from the Ref.[51] and is slightly different from it. The positions and directions of all the twelve thrusters with respect to the body-fixed reference frame are given in Table 1.

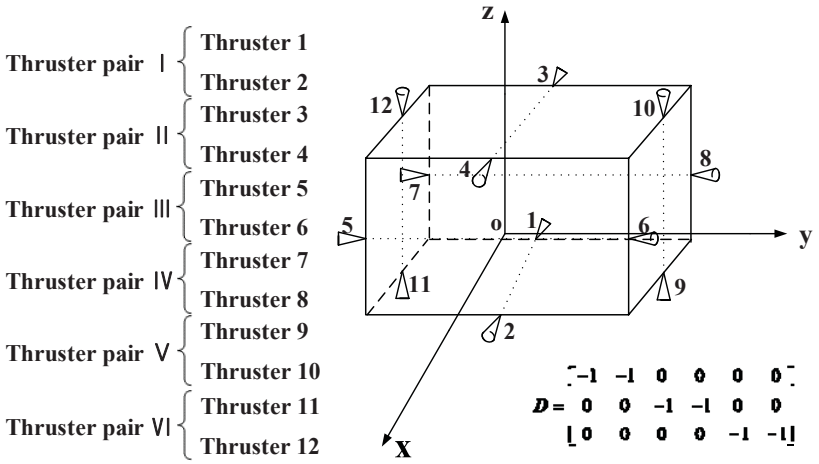

Fig. 2 Distribution schematics of six thruster pairs and the thrust distribution matrix

Table 1 Positions and direction of the thrusts in the body frame of the chaser satellite

Thruster pair	Thruster number	Thruster position	Thrust direction	Thruster number	Thruster position	Thrust direction
Ⅰ	1	$[0\ 0\ -0.8]^T$	$[1\ 0\ 0]^T$	2	$[0\ 0\ -0.8]^T$	$[-1\ 0\ 0]^T$
Ⅱ	3	$[0\ 0\ 0.8]^T$	$[1\ 0\ 0]^T$	4	$[0\ 0\ 0.8]^T$	$[-1\ 0\ 0]^T$
Ⅲ	5	$[0.7\ 0\ 0]^T$	$[0\ 1\ 0]^T$	6	$[0.7\ 0\ 0]^T$	$[0\ -1\ 0]^T$

Ⅳ	7	$[-0.7\ 0\ 0]^{\mathrm{T}}$	$[0\ 1\ 0]^{\mathrm{T}}$	8	$[-0.7\ 0\ 0]^{\mathrm{T}}$	$[0\ -1\ 0]^{\mathrm{T}}$
Ⅴ	9	$[0\ 0.7\ 0]^{\mathrm{T}}$	$[0\ 0\ 1]^{\mathrm{T}}$	10	$[0\ 0.7\ 0]^{\mathrm{T}}$	$[0\ 0\ -1]^{\mathrm{T}}$
Ⅵ	11	$[0\ -0.7\ 0]^{\mathrm{T}}$	$[0\ 0\ -1]^{\mathrm{T}}$	12	$[0\ -0.7\ 0]^{\mathrm{T}}$	$[0\ 0\ -1]^{\mathrm{T}}$

The mass of the chaser spacecraft without propellant is 700kg and the initial propellant mass $m_{p(0)}$ is 300kg. According the mass flow in Eq.(15), the propellant mass m_p is obtained as

$$m_p = m_{p(0)} - \sum_{i=1}^{\mathrm{VI}} \left[\int_0^t \left| F_{ci}(t) \right| / \left(I_{sp} g \right) dt \right] \tag{62}$$

The other simulation parameters of the two spacecrafts are given in Table 2.

Table 2 Simulation parameters

Parameters name	Parameters value	Units
$\boldsymbol{J}_t$	diag([1500,1800,2100])	$\mathrm{kg \cdot m^2}$
$[\Omega, i_0, \omega_0]$	$[30, 45, 10]$	deg
a	7200	km
e	0.005	—
t_p	0	s
μ	3.980044×10^5	$\mathrm{km^3 / s^2}$
$\boldsymbol{\omega}_t$	$[-0.75, 0.5, 0.75]^{\mathrm{T}}$	deg/s
$[q_{t0} \quad \boldsymbol{q}_{t0}]^{\mathrm{T}}$	$[0.548, 0.6, -0.5, 0.3]^{\mathrm{T}}$	—
$m_{c(0)}$	1000	kg
I_{SP}	4500	sec

Case A. Comparison without thruster faults or external disturbance

In this case, the initial position of the chaser spacecraft in the LOS coordinate frame have been set to $[\rho_0, \psi_0, \theta_0]^{\mathrm{T}} = \left[100\mathrm{m}, \left(0.6 \times 180^{\circ} \right) / \pi, -\left(0.4 \times 180^{\circ} \right) / \pi \right]^{\mathrm{T}}$, with no initial relative velocity. In an actual rendezvous and docking mission, the chaser spacecraft should approach the target spacecraft along a prescribed docking axis. This requirement can be easily met using the LOS based equation of relative motion (12), especially for a tumbling target. As described in Section 2, the -X axis of the target is chosen as the docking axis. The chaser spacecraft first approaches the -X axis of the target and then keeps the relative range as 60m and 30m in turn for a fly-around. The total rendezvous process is completed in 1500s, and the distance between the

center of the target and the docking device is set to be 10m. Thus, the desired distance ρ_d is defined as

$$\rho_d = \begin{cases} 60\text{m} & 0\text{s} \\ 30\text{m} & 500\text{s} \\ 10\text{m} & 1000\text{s} \end{cases} \tag{63}$$

The control gains for the two controllers are given in Table 3 and selected by trial-and-error until a good tracking performance is obtained.

Table 3 The parameters used in the simulation

Controllers	Control parameters
Fixed-time based finite-time controller in Eq.(25)	$\boldsymbol{\alpha}_1 = \text{diag}([0.1, 0.06, 0.05])$, $\boldsymbol{\beta}_1 = \text{diag}([0.075, 0.05, 0.05])$ $\boldsymbol{\alpha}_2 = \text{diag}([0.06, 0.06, 0.06])$, $\boldsymbol{\beta}_2 = \text{diag}([0.06, 0.06, 0.05])$ $p_1 = 0.75$, $g_1 = 1.2$, $k_1 = 1.1$, $p_2 = 0.8$, $g_2 = 1.2$
Adaptive fixed-time based finite-time controller in Eq.(31)	$\boldsymbol{\alpha}_1 = \text{diag}([0.1, 0.06, 0.05])$, $\boldsymbol{\beta}_1 = \text{diag}([0.075, 0.05, 0.05])$ $\boldsymbol{\alpha}_3$=diag$([0.06, 0.06, 0.06])$, $\boldsymbol{\beta}_3 = \text{diag}([0.06, 0.06, 0.05])$ $p_1 = 0.75$, $g_1 = 1.2$, $k_1 = 1.1$, $p_2 = 0.8$, $g_2 = 1.2$ $\theta_1 = \theta_2 = 2$, $\sigma_1 = 0.003$, $\sigma_2 = 100$, $\hat{d}(0) = 1$, $\hat{\boldsymbol{\Theta}}(0) = [0, 0, 0, 0, 0, 0]^{\mathrm{T}}$

In addition, using the mathematical formula of convergence time in Eq.(26) and the parameters in Table 3, the upper bound of settling time can be estimated as follows

$$T \le \frac{1}{0.05^{1.1} \times (1 - 0.75 \times 1.1)} + \frac{1}{0.05^{1.1} \times (1.2 \times 1.1 - 1)} + \frac{1}{0.06 \times (1 - 0.8)} + \frac{1}{2^{1-1.2} \times 0.05 \times (1.2 - 1)} < 450\text{s} \tag{64}$$

which means the chaser spacecraft can rendezvous with target within the specified time limit(i.e. 500 sec, scheduled in Eq.(63)) The comparative simulations are conducted and the results are shown in Figs. 3 to 7. Figure 3 to 4 show that both of the two controllers have good performance and the adaptive fixed-time based finite time controller has better control precision. Both settling time for the relative position are identical, i.e. 100s, which can be seen from Fig.5. Figure 6 shows that the actual control forces are within their maximum

allowable limit, i.e. 10N; both of the controllers are continuous, and chatter-free. Since thrusters 3 and 4, thrusters 7 and 8 and thrusters 11 and 12 have the same forces as the thrusters 1 and 2, thruster 5 and 6 and thrusters 9 and 10 respectively, their forces are not plotted. Figure 7 shows that the proposed adaptive fixed-time controller consumes less propellant mass than the one given by Eq.(25).

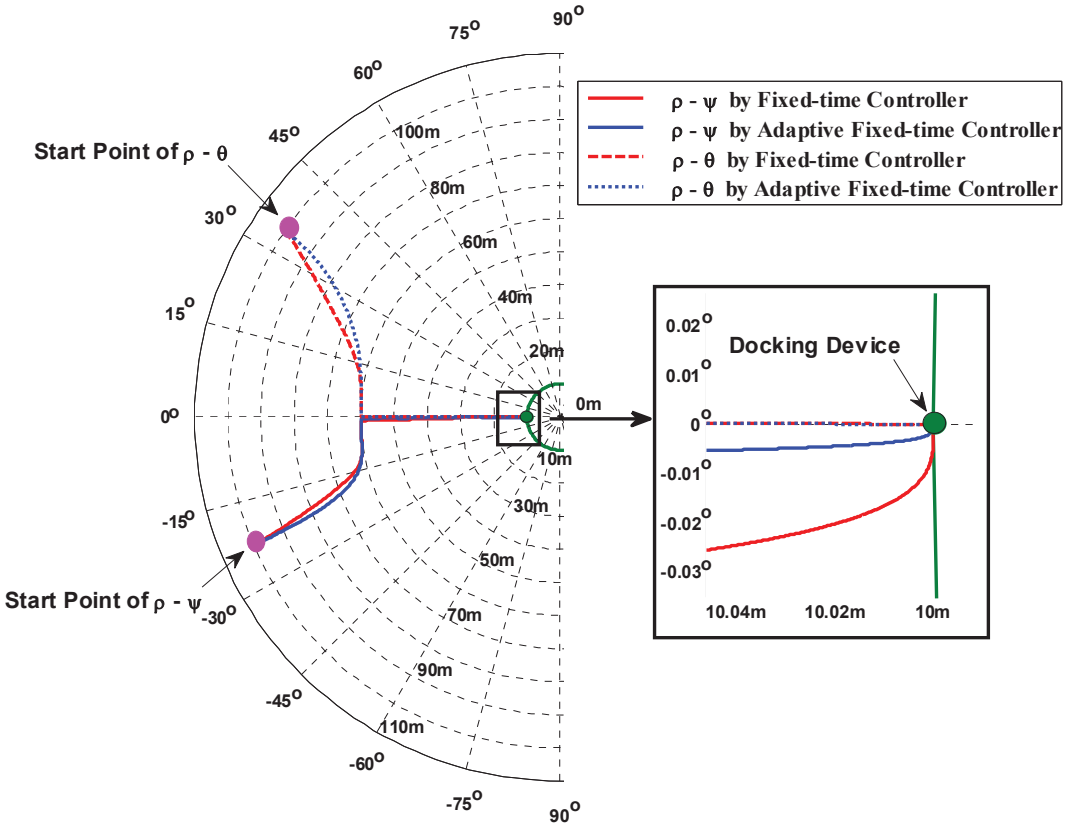

Fig. 3 Time response of the position states (ρ, ψ, θ) in polar coordinates without thruster faults or disturbance.

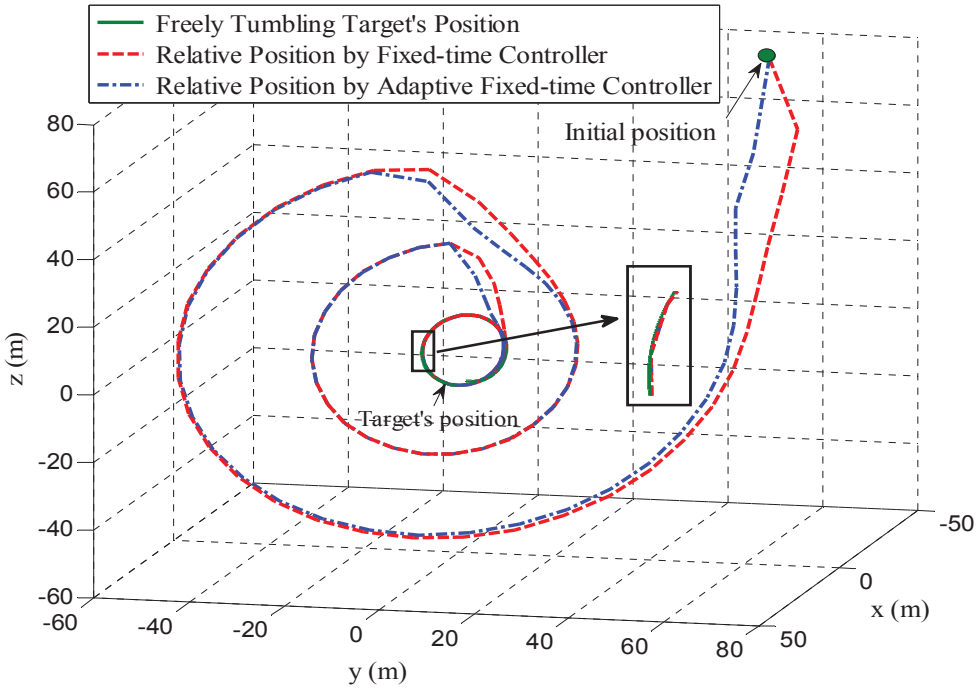

Fig. 4 Chaser spacecraft's position in the target's orbital coordinate frame without thruster faults or disturbance.

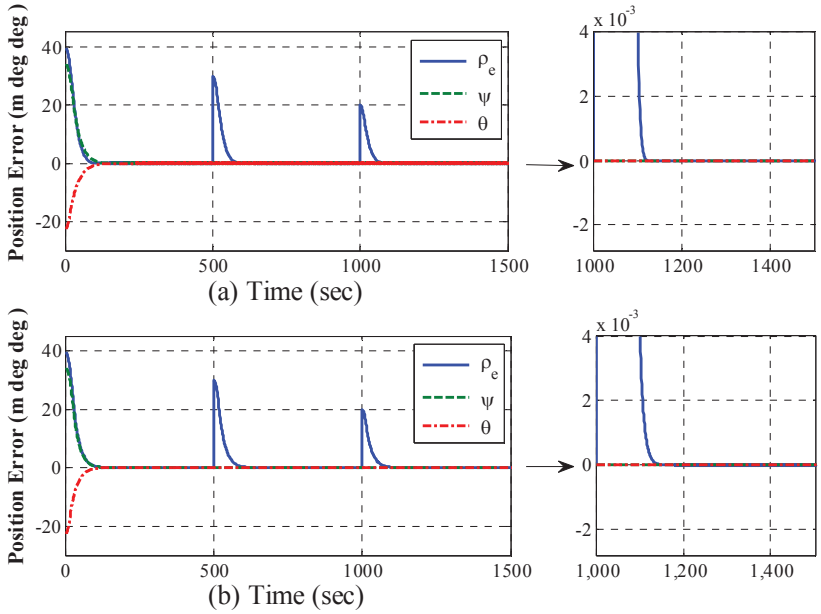

Fig. 5 Time response of the position errors (ρ_e, ψ, θ) without thruster faults or disturbance: (a) the fixed-time based finite time controller in Eq.(25) (b) the adaptive fixed-time based finite time controller in Eq.(31).

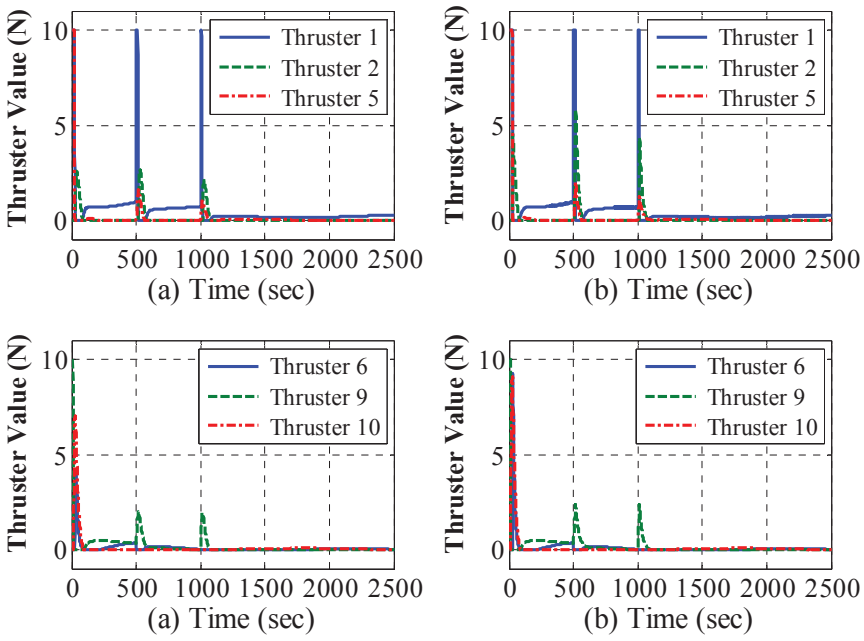

Fig. 6 Time response of the force of each thruster without thruster faults or disturbance: (a) the fixed-time based finite time controller in Eq.(25) (b) the adaptive fixed-time based finite time controller in Eq.(31).

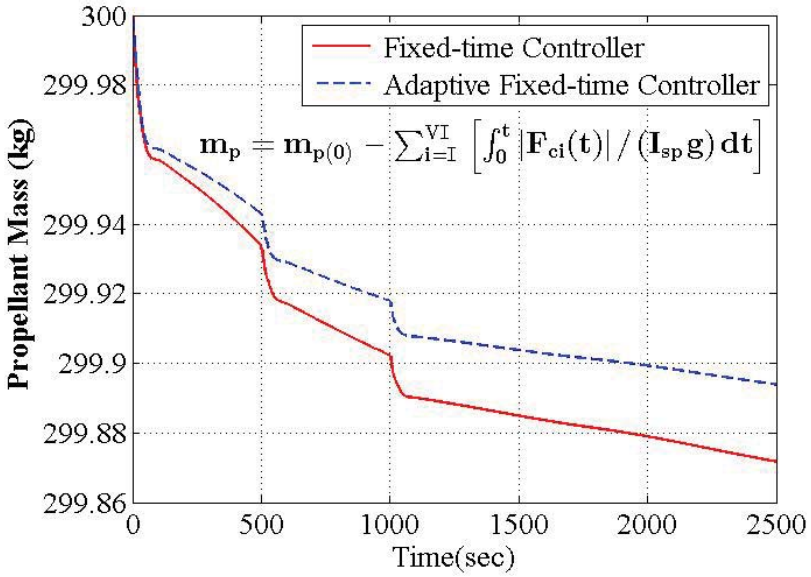

Fig.7 Propellant mass for the two controllers without thruster faults or disturbance.

Case B. Comparison with thruster faults and disturbance

In this case, severe thruster faults are considered, and the fault scenario is given by

$$E_1 = E_2 = E_5 = E_6 = \begin{cases} 0 & \text{if } t \le 100 \\ 0.2 & \text{otherwise} \end{cases}, \quad E_3 = E_4 = E_7 = E_8 = \begin{cases} 0 & \text{if } t \le 500 \\ 0.5 & \text{otherwise} \end{cases}, \quad E_9 = E_{10} = 0.1, \quad E_{11} = E_{12} = 0 \quad (65)$$

$$\bar{F}_{C3}=\bar{F}_{C4}=\bar{F}_{C5}=\bar{F}_{C6}=\begin{cases}0.5 & if\ \ t\le 500\\ 0 & \text{otherwise}\end{cases},\quad \bar{F}_{Ci}=0\ \ (\text{i}=1,2,7,8,9,10,11,12) \tag{66}$$

According to Eq.(1) and Eq.(13), $\boldsymbol{d}_L$ has the following form

$$\boldsymbol{d}_L=-m_c\boldsymbol{R}_{Lt}\boldsymbol{J}_t^{-1}\boldsymbol{d}_t\times\boldsymbol{\rho}+m_c\boldsymbol{a}_{J2t}-m_c\boldsymbol{a}_{J2c}-m_c\boldsymbol{a}_w \tag{67}$$

where $\boldsymbol{d}_t=10^{-5}$ Nm and $\boldsymbol{a}_w=\left[3\cos(0.2t)+1\quad 1.5\sin(0.2t)+3\cos(0.2t)+2\quad 3\sin(0.2t)+3\right]^{\mathrm{T}}\times10^{-5}$ m/s^2 [42]. In addition, we also consider the uncertain mass of chaser spacecraft and the uncertain inertia of target spacecraft where the variation are less than 3% and 8% respectively. The control parameters remain those given in Table 2, and the results are shown in Figs. 8 to 12. Figures 8 and 9 show the macroscopic time responses for the two controllers, and it is clear that the adaptive fixed-time controller has better adaptability to the thruster faults and disturbance. Figure 10 shows that the fixed-time controller in Eq.(25) has the faster transient response and the adaptive fixed-time controller has the higher accuracy However, the proposed controller in Eq.(31) consumes less propellant mass, as shown in Figs. 11 and 12. The system performance of the controller in Eq.(25) is significantly degraded by thruster faults and disturbance. The results presented demonstrate the desirable features of the proposed adaptive fixed-time controller, such as finite-time convergence, fault tolerant capability, and robustness to external disturbances.

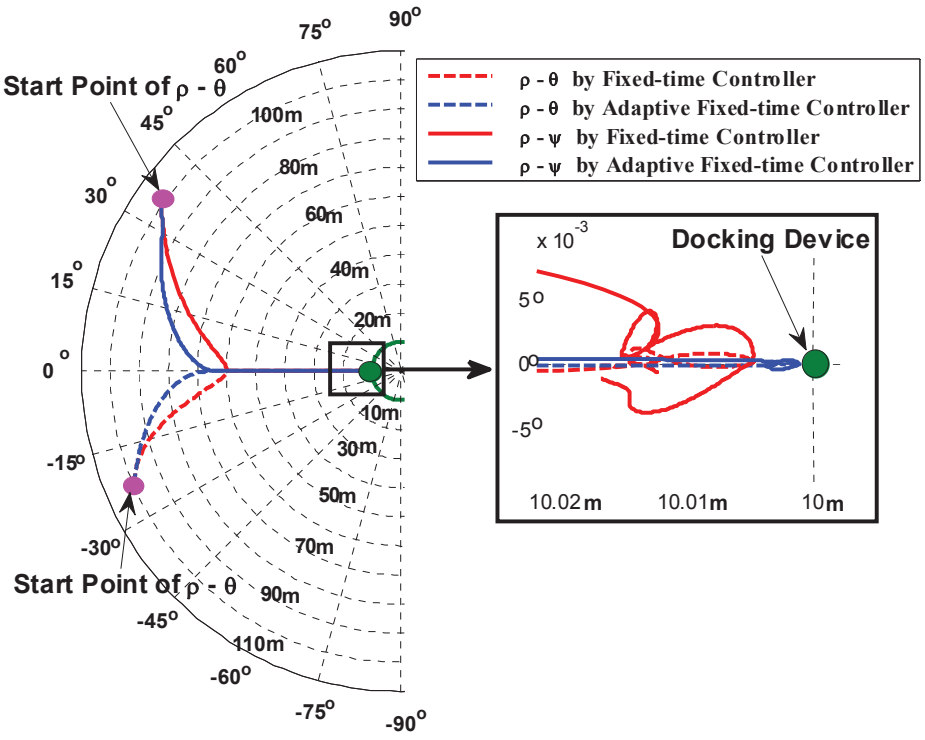

Fig. 8 Time response of the position states (ρ, ψ, θ) in polar coordinates with thruster faults and disturbance.

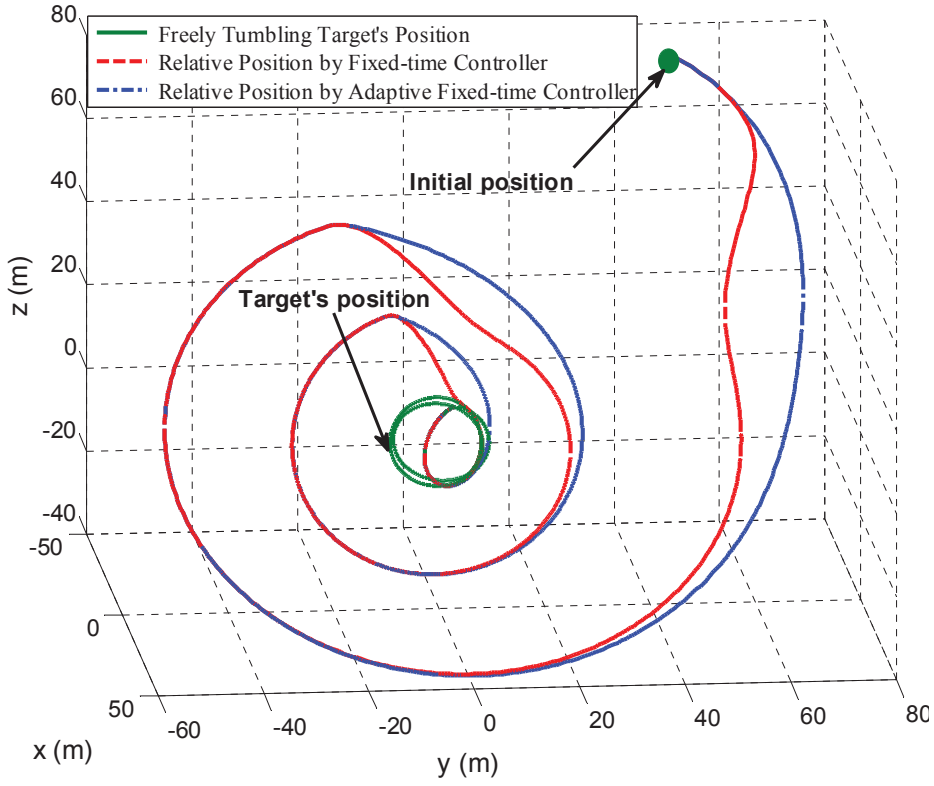

Fig. 9 Chaser spacecraft's position in the target's orbital coordinate frame with thruster faults and disturbance.

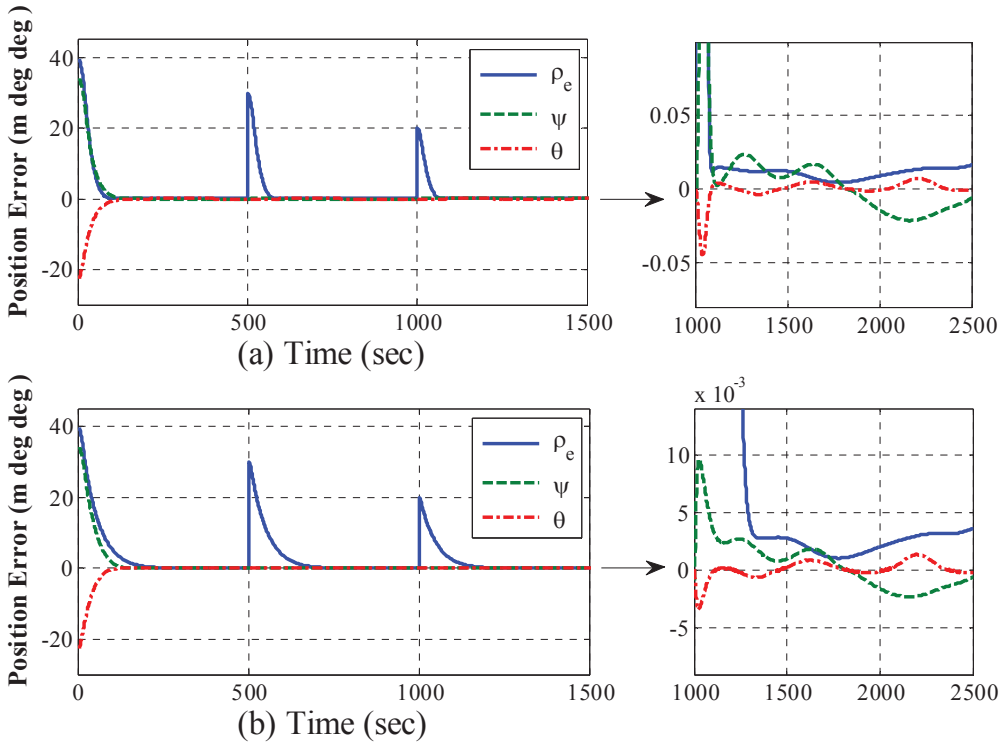

Fig. 10 Time response of the position errors (ρ_e, ψ, θ) with thruster faults and disturbance: (a) the fixed-time controller in Eq.(25) (b) the adaptive fixed-time controller in Eq.(31).

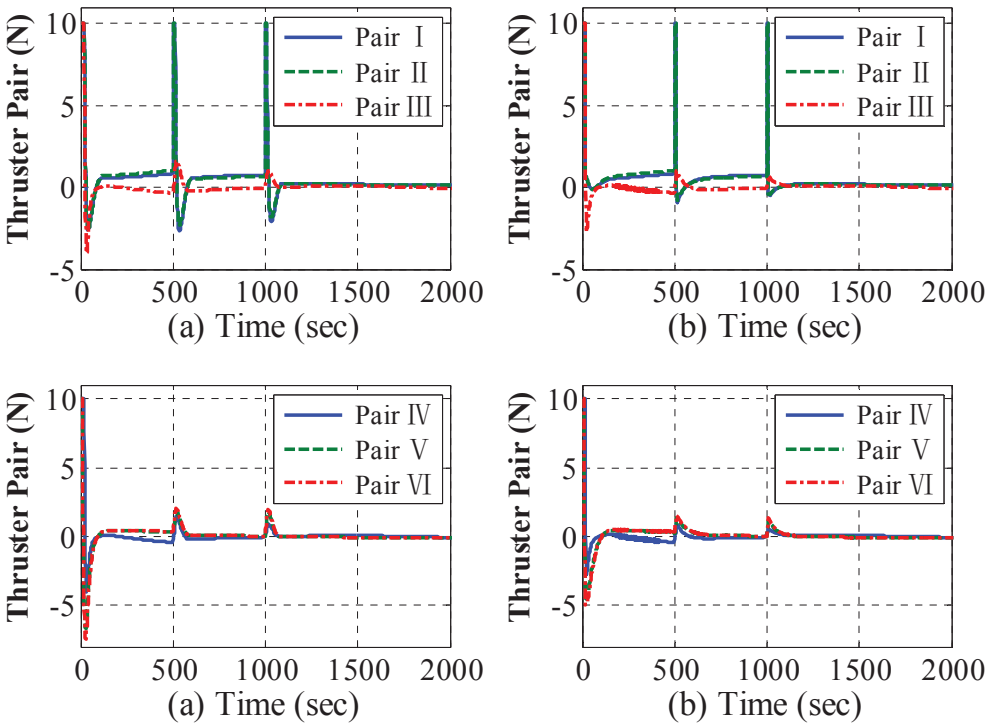

Fig. 11 Time response of the force of each thruster pair with thruster faults and disturbance: (a) the fixed-time controller in Eq.(25) (b) the adaptive fixed-time controller in Eq.(31).

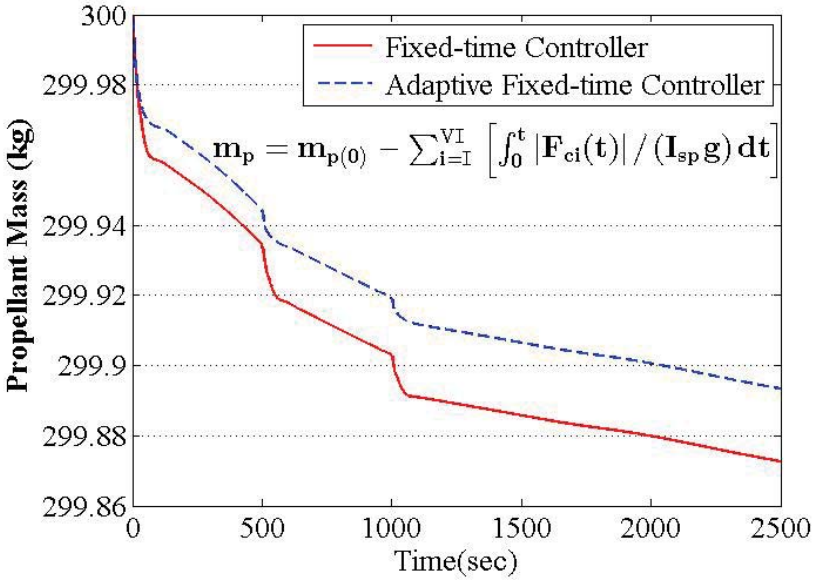

Fig.12 Propellant mass for the two controllers with thruster faults and disturbance.

Case C. Comparison with thruster faults, disturbance , sensor noise and new initial conditions

In this case, to further examine the adaptability of the two control schemes, new initial conditions $\left[\rho_0, \psi_0, \theta_0\right]^{\mathrm{T}} = \left[100\mathrm{m}, 2\times 180^\circ/\pi, -0.8\times 180^\circ/\pi\right]^{\mathrm{T}}$ and $\rho_d = \begin{cases} 80\mathrm{m} & 0\mathrm{s} \\ 10\mathrm{m} & 500\mathrm{s} \end{cases}$ have been considered. The control parameters remain those given in Table 3, and the thruster faults and disturbance remain the same as in Case B. Moreover, the sensor noise has been taken into consideration and drawn from the mixture of zero-mean Gaussian probability distributions, defined by the probability density function $p(\zeta) = \left[1/\left(\sigma\sqrt{2\pi}\right)\right]\exp\left[-(\zeta/\sigma)^2/2\right]$, where σ are the standard deviations of the individual Gaussian distributions. The standard deviation σ is chosen according to the following Table 4[52].

Table 4. Rendezvous navigation sensor noise

Measurement	Standard deviation (σ)
Rang (ρ), m	1.518×10^{-2}
Elevation (ψ), deg	2.787×10^{-3}
Azimuth (θ), deg	1.404×10^{-3}

Figures 13 to 17 show that high control precision and good performance are still obtained, and no significant amount of oscillations occurred even under severe faults for the proposed controller. Note especially that the settling time of the proposed controllers in Eq.(25) and Eq.(31) are nearly the same as that in Case B, which is to say both of the proposed fixed-time controllers have great robustness to different initial conditions. Severe oscillation are excited due to the existence of sensor noise, while both of the control accuracy of the two fixed-time controllers satisfy the rendezvous requirements well, i.e. 0.05m and 0.05 deg. In addition the controller in Eq.(31) is little better than controller in Eq.(25) in the control precision and the loss of propellant mass, shown in Fig. 13 and Fig.17.

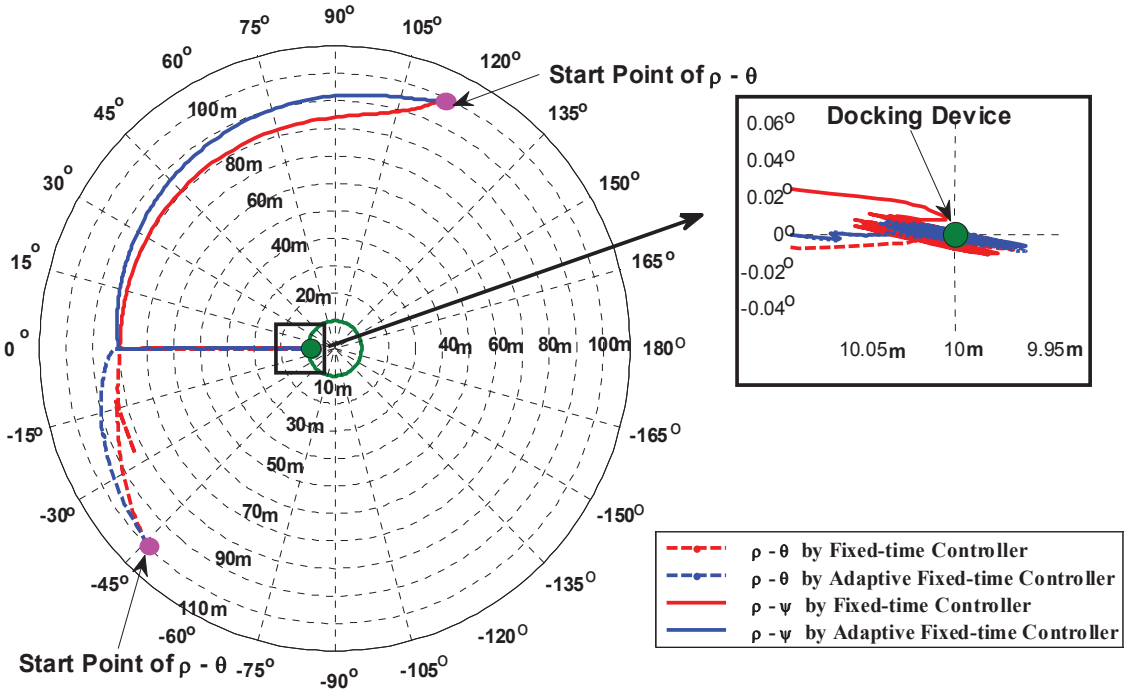

Fig. 13 Time response of the position states (ρ, ψ, θ) in polar coordinates with new initial conditions and noise.

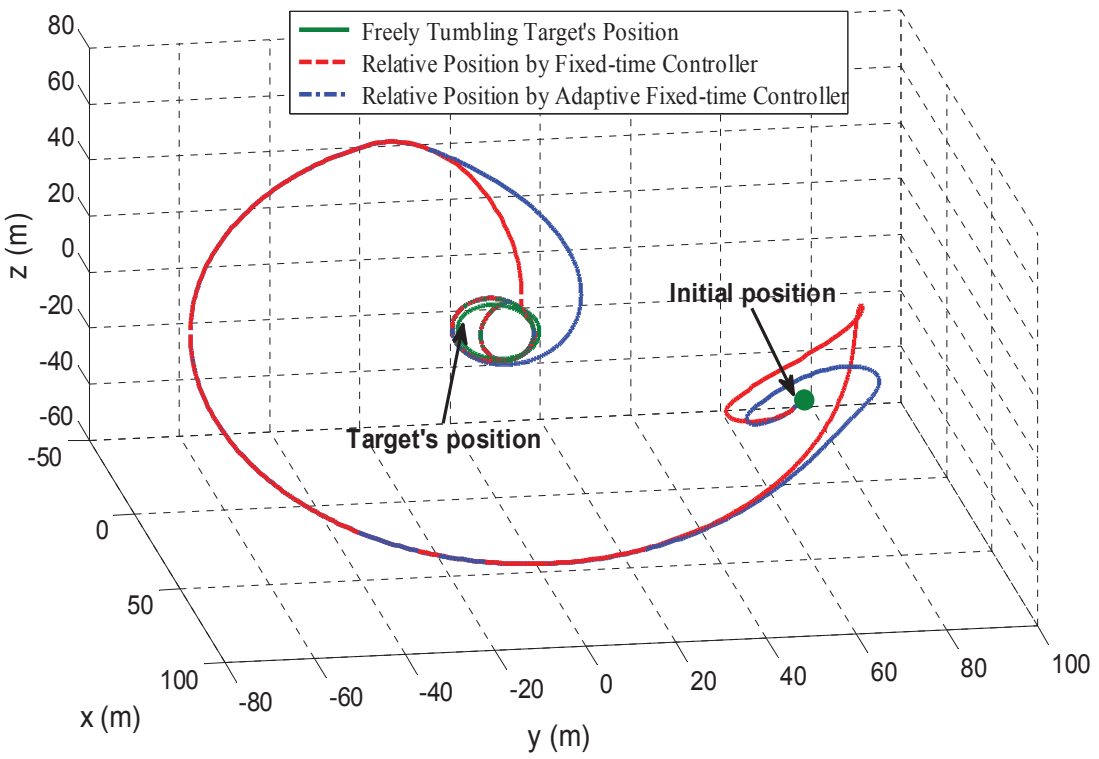

Fig. 14 Chaser spacecraft's position in the target's orbital coordinate frame with new initial conditions.

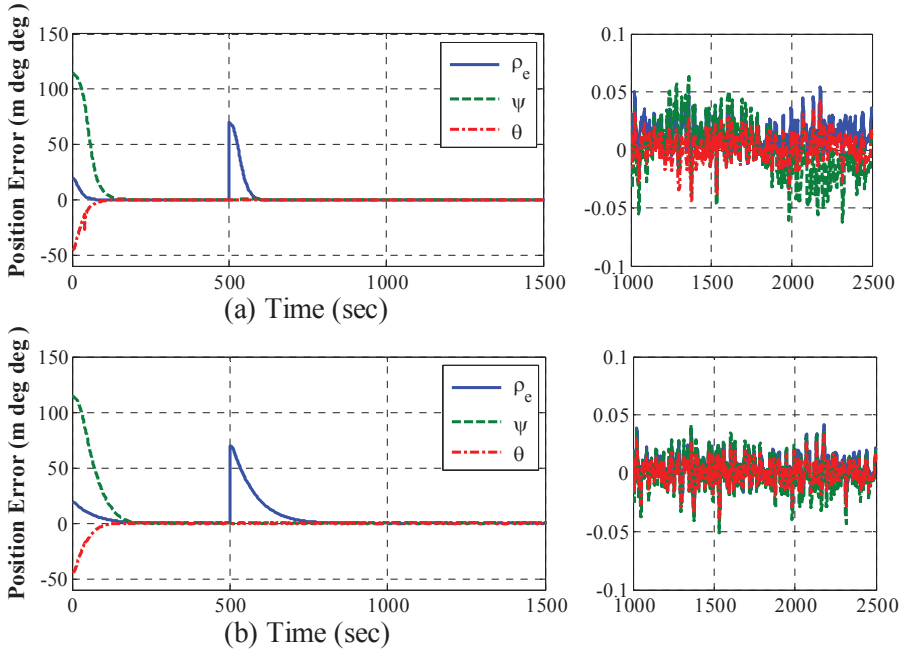

Fig. 15 Time response of the position errors (ρ_e, ψ, θ) with new initial conditions: (a) the fixed-time controller in Eq.(25) (b) the adaptive fixed-time controller in Eq.(31).

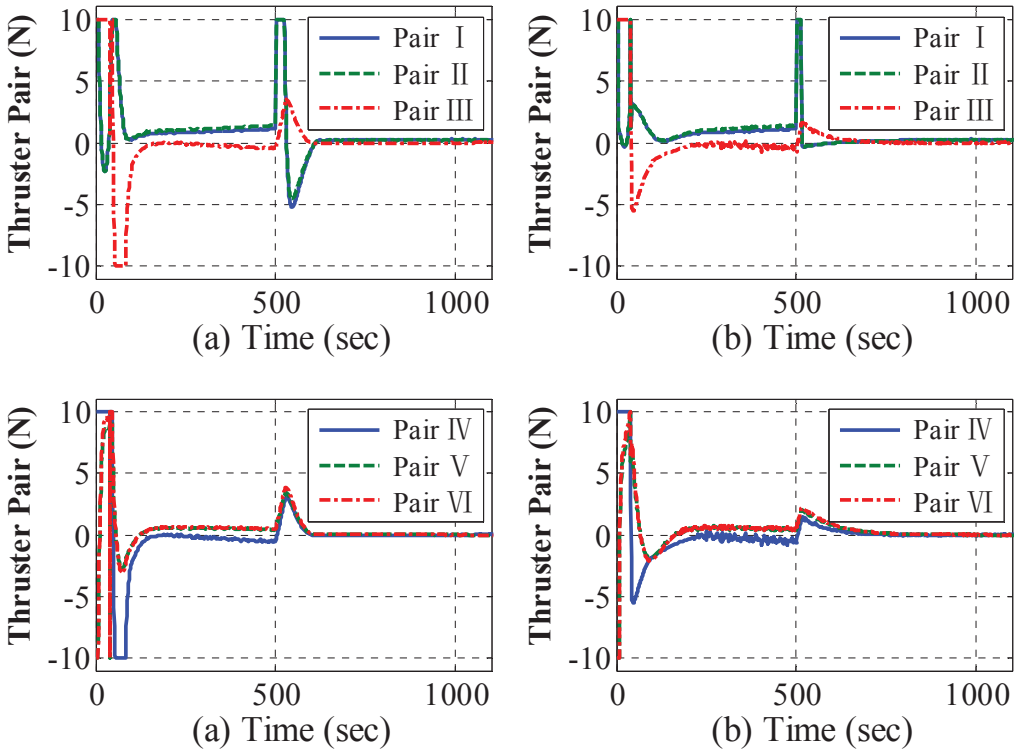

Fig. 16 Time response of the force of each thruster pair with new initial conditions: (a) the fixed-time controller in Eq.(25) (b) the adaptive fixed-time controller in Eq.(31).

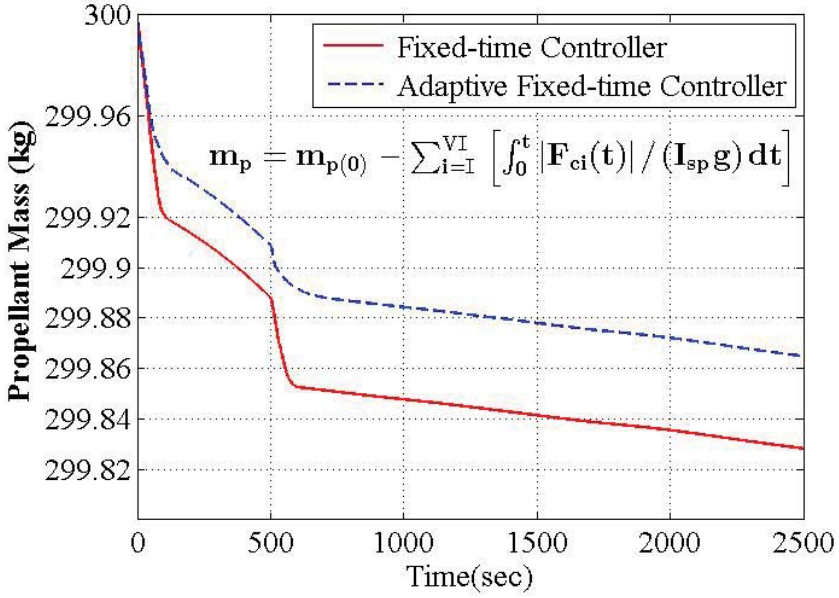

Fig.17 Propellant mass for the two controllers with new initial conditions.

Summarizing all of the cases, both the fixed-time controller in Eq.(25) and the adaptive fixed-time based finite time controller in Eq.(31) are able to successfully accomplish rendezvous and docking with high attitude

pointing accuracy and stability, when thruster faults and external disturbances are not present. However, the controller in Eq.(31) has much better adaptability in the presence of external disturbances, measurement noise, different initial conditions and thruster faults, both in theory and in simulation. In addition, some simulations were performed using different control parameters, disturbance inputs and even combination of thrusters faults. These results show that closed-loop system rendezvous control is accomplished in spite of these undesired effects in the system. Moreover, the flexibility in the choice of the control parameters can be utilized to obtain desirable performance while meeting constraints on the control magnitude.

7. Conclusion

In this paper, dynamic equations are derived for rendezvous and docking with a tumbling target. Novel fixed-time fault tolerant controllers are proposed to perform the challenging and complicated rendezvous mission with a non-cooperative spacecraft. In contrast to the existing finite-time control literature, the fixed-time controllers are independent of initial conditions and have more rapid convergence and higher accuracy. The performance of the proposed controllers is examined through numerical simulation. It is shown that the proposed adaptive fixed-time controller has faster convergence and better fault-tolerant capability with higher accuracy than the general fixed-time controller. This conclusion is valid with the assumption that the velocity of target is known, although an actual non-cooperative target's speed would be unknown. The results presented in this paper are given for a particular numerical simulation; further experimental testing would be required to reach any conclusion about the efficacy of the control and adaptation laws for a real mission.

ACKNOWLEDGMENTS

This work was supported partially by National Natural Science Foundation of China (Project No.61273175, 61522301), Program for New Century Excellent Talents in University (NCET-11-0801), Heilongjiang Province Science Foundation for Youths (QC2012C024), and Research Fund for Doctoral Program of Higher Education of China (20132302110028). The authors greatly appreciate the above financial support. The authors would also

like to thank the associate editor and reviewers for their valuable comments and constructive suggestions that helped to improve the paper significantly.

References

[1] Newkirk, D., "Repair of Salyut 7," *IEEE Aerospace and Electronic Systems Magazine*, Vol. 3, No 9, 1988, pp. 9-11.

[2] Clohessy, W. H., and Wiltshire, R. S., "Terminal Guidance System For Satellite Rendezvous," *Journal of Aerospace Science*, Vol. 27, No. 9, 1960, pp. 653-658.

[3] Schaub, H., and Junkins, J. L., *Analytical Mechanics of Space Systems*, AIAA Education Series, AIAA, Reston, VA, 2003.

[4] Tschauner, J., Hempel, P., "Rendezvous With A Target In An Elliptical Orbit," *Acta Astronautica,* Vol. 11, No. 2, 1965, pp. 104–109.

[5] Yu, S., "Terminal Spacecraft Coplanar Rendezvous Control," *Journal of Guidance, Control, and Dynamics*, Vol. 18, No. 4, 1995, pp. 838-842.

[6] Yu, S., "Autonomous Rendezvous In Elliptical Orbits," *Acta Astronautica*, Vol. 41, No. 2, 1997, pp. 95-101.

[7] Yu, S., "Control Schemes For Terminal Space Rendezvous," *Acta Astronautica*, Vol. 43, No. 7, 1998, pp. 349-354.

[8] Gim, D. W., Alfriend, K. T., "State Transition Matrix Of Relative Motion For The Perturbed Noncircular Reference Orbit," *Journal of Guidance, Control, and Dynamics,* Vol. 26, No. 6 2003, pp. 956–971.

[9] Ross, I. M., "Linearized Dynamic Equations For Spacecraft Subject To J2 Perturbations," *Journal of Guidance, Control, and Dynamics,* Vol. 26, No. 4, 2003, pp. 57–659.

[10] Mokuno, M., Kawano, I., and Suzuki, T., "In-Orbit Demonstration Of Rendezvous Laser Radar For Unmanned Autonomous Rendezvous Docking," *IEEE Transactions on Aerospace and Electronic Systems,* Vol. 40, No. 2, 2004, pp. 617-626.

[11] Gao, H. J, Yang, X. B, and Shi, P., "Multi-Objective Robust H_∞ Control Of Spacecraft Rendezvous," *IEEE Transactions on Control Systems Technology*, Vol.17, No.4, 2009, pp.794-802.

[12] Wu, S., Wu, Z., Radice, G., and Wang, R., "Adaptive Control For Spacecraft Relative Translation With Parametric Uncertainty," *Aerospace Science and Technology,* Vol. 31, No. 1, 2013, pp. 53-58.

[13] Singla, P., Subbarao, K., and Junkins, J. L., "Adaptive Output Feedback Control For Spacecraft Rendezvous And Docking Under Measurement Uncertainty," *Journal of Guidance, Control, and Dynamics,* Vol. 29, No. 4, 2006, pp.

892-902.

[14] Yoon, H., Agrawal, B., N., “Novel Expressions Of Equations Of Relative Motion And Control In Keplerian Orbits,” *Journal of guidance, control, and dynamics*, Vol. 32, No. 2, 2009, pp. 664-669.

[15] Yoon, H., Eun, Y., Park, C.. “Adaptive Tracking Control Of Spacecraft Relative Motion With Mass And Thruster Uncertainties,” *Aerospace Science and Technology*, Vol. 34, No. 1, 2014, pp. 75-83.

[16] Zhang, D. W., Song S M, Pei R. “Safe Guidance For Autonomous Rendezvous And Docking With A Non-Cooperative Target,” *AIAA Guidance, Navigation, and Control Conference*, 2010 pp. 1-19.

[17] Lu, W., Geng, Y. H., Chen, X. Q., and Zhang, F., “Relative Position And Attitude Coupled Control For Autonomous Docking With A Tumbling Target,” *International Journal of Control and Automation*, Vol. 4, No. 4, 2011, pp. 1-22.

[18] Di Cairano, S., Park, H., Kolmanovsky, I., “Model Predictive Control Approach for Guidance of Spacecraft Rendezvous And Proximity Maneuvering,” *International Journal of Robust and Nonlinear Control*, Vol 22, No 12, 2012, p 1398-1427.

[19] Liang, J. X., and Ma, O., “Angular Velocity Tracking for Satellite Rendezvous And Docking,” *Acta Astronautica*, Vol 69, No 11-12, 2011, pp. 1019-1028.

[20] Michael, J., Chudej, K., Gerdts, M., and Pannek, J. “Optimal Rendezvous Path Planning to An Uncontrolled Tumbling Target,” *19th IFAC Symposium on Automatic Control in Aerospace, ACA 2013 - Proceedings*, Vol 19, No 1, 2013, pp. 347-352.

[21] Bhat, S., and Bernstein, D., "Finite-Time Stability of Continuous Autonomous Systems," *SIAM Journal on Control and Optimization*, Vol. 38, No. 3, 2000, pp. 751-766.

[22] Bhat, S. P., and Bernstein, D. S, "Geometric Homogeneity with Applications to Finite-Time Stability," *Mathematics of Control, Signals, and Systems*, Vol. 17, No. 2, 2005, pp. 101-127.

[23] Bhat, S. P., and Bernstein, D. S, "Continuous Finite-Time Stabilization of The Translational And Rotational Double Integrators," *IEEE Transactions on Automatic Control*, Vol. 43, No. 5, 1998, pp. 678-682.

[24] Sun, H., Li, S. and Fei, S., "A Composite Control Scheme for 6DOF Spacecraft Formation Control," *Acta Astronautica*, Vol. 69, No. 7, 2011, pp. 595-611.

[25] Hui, L. and Li, J., "Terminal Sliding Mode Control for Spacecraft Formation Flying." *IEEE Transactions on Aerospace and Electronic Systems,* Vol. 45, No. 3, 2009, pp. 835-846.

[26] Lu, K. and Xia, Y., "Finite-Time Fault-Tolerant Control for Rigid Spacecraft with Actuator Saturations," *IET Control Theory and Applications*, Vol. 7, No. 11, 2013, pp. 1529-1539.

[27] Polyakov, A., "Nonlinear Feedback Design for Fixed-Time Stabilization of Linear Control Systems," *IEEE Transactions on Automatic Control*, Vol. 57, No. 8, 2012, pp. 2106-2110.

[28] Polyakov, A., Efimov, D., and Perruqetti, W., "Finite-Time And Fixed-Time Stabilization: Implicit Lyapunov Function Approach" *Automatica*, Vol. 51, 2015, pp. 332-340.

[29] Levant, A., "On Fixed And Finite Time Stability in Sliding Mode Control," *2013 IEEE 52nd Annual Conference on Decision and Control*, pp. 4260-4265.

[30] Chen, W. and Saif, M., "Observer-Based Fault Diagnosis of Satellite Systems Subject to Time-Varying Thruster Faults," *Journal of Dynamic Systems Measurement and Control*, Vol. 129, No. 3, 2007, pp. 352-356.

[31] Patton, R., Uppal, F., Simani, S., and Polle, B., "Robust FDI Applied to Thruster Faults of A Satellite System," *Control Engineering Practice*, Vol. 18, No. 9, 2010, pp. 1093-1109.

[32] Fonod, R., Henry, D., Charbonnel, C., and Bornschlegl, E., "Position And Attitude Model-Based Thruster Fault Diagnosis: A Comparison Study," *Journal of Guidance Control and Dynamics*, Vol. 38, No. 6, 2015, pp. 1012-1026.

[33] Fonod, R., Henry, D., Bornschlegl, E., and Charbonnel, C., "Thruster Fault Detection, Isolation and Accommodation for An Autonomous Spacecraft," In 19th IFAC world congress Cap Town, South Africa, 2014, pp. 10543-10548.

[34] Henry, D., Olive, X., and Bornschlegl, E., "A Model-Based Solution for Fault Diagnosis of Thruster Faults: Application to The Rendezvous Phase of The Mars Sample Return Mission," In 4th European conference for aerospace sciences (EUCASS), Russian Federation: St. Petersburg, 2011.

[35] Henry, D., "Fault Diagnosis of Microscope Satellite Thrusters using Hinf/H- Filters," *Journal of Guidance, Control and Dynamics*, Vol. 31, No. 3, pp. 699-711.

[36] Qian, M., and Jie, C., "Robust Fault-Tolerant Control for A Class Of Spacecraft Rendezvous System: Actuator Fault Case," *ICIC Express Letters, Part B: Applications*, Vol. 1, No. 2, 2010, pp. 255-560.

[37] Marwaha, M., and Valasek, J., "Fault−tolerant Control Allocation for Mars Entry Vehicle using Adaptive Control," *International Journal of Adaptive Control and Signal Processing*, 2011, Vol. 25, No. 2, pp.95-113.

[38] Hu, Q., Li, B., Wang, D., and Kee Poh, E., "Velocity-Free Fault-Tolerant Control Allocation for Flexible Spacecraft with Redundant Thrusters," *International Journal of Systems Science,* Vol. 46, No. 6, 2015, pp. 976-992.

[39] Hu, Q., and Xiao, B., "Adaptive Fault Tolerant Control Using Integral Sliding Mode Strategy With Application To Flexible Spacecraft," *International Journal of Systems Science,* Vol. 44, No. 12, 2013, pp. 2273-2286.

[40] Zhang, Y., and Jiang, J., "Bibliographical Review On Reconfigurable Fault-Tolerant Control Systems," *Annual Reviews in Control,* Vol. 32, No. 2, 2008, pp. 229-252.

[41] Jiang, J., and Yu, X., "Fault-Tolerant Control Systems: A Comparative Study Between Active And Passive Approaches," *Annual Reviews in Control,* Vol. 36, No. 1, 2013, pp.60-72.

[42] Okasha, M., and Newman, B., "Relative Motion Guidance, Navigation And Control For Autonomous Orbital Rendezvous," *AIAA Guidance, Navigation, and Control Conference 2011*, 2011.

[43] Vallado, D. A., "Fundamentals of Astrodynamics and Applications", Microcosm Press, EI Segundo, California, 2nd Edition, 2001.

[44] Xu, Y. J., Tatsch, A., and Fitz-Coy, N. G., "Chattering Free Sliding Mode Control for a 6 DOF Formation Flying Mission," *Collection of Technical Papers - AIAA Guidance, Navigation, and Control Conference*, Vol 8, 2005, pp. 6210-6219.

[45] Z. Zhu, Y. Xia, and M. Fu, "Attitude Stabilization Of Rigid Spacecraft With Finite-Time Convergence," *International Journal of Robust and Nonlinear Control,* Vol. 21, No. 6, 2011, pp. 686-702.

[46] Yu, S., Yu, X., Shirinzadeh, B., and Man, Z, "Continuous Finite-Time Control For Robotic Manipulators With Terminal Sliding Mode," *Automatica*, Vol. 41, No. 11, 2005, pp. 1957-1964.

[47] Qian, C., and Lin, W., "A Continuous Feedback Approach To Global Strong Stabilization Of Nonlinear Systems," *IEEE Transactions on Automatic Control*, Vol. 46, No. 7, 2001, pp. 1061-1079.

[48] Li, J, Qian, C.J, and Frye, M.T., "A Dual-Observer Design For Global Output Feedback Stabilization Of Nonlinear Systems With Low-Order And High-Order Nonlinearities", *International Journal of Robust and Nonlinear Control*, Vol, 19, No. 15, 2009, pp. 1697-1720.

[49] Hu, Q.L., and Xiao B., "Adaptive Fault Tolerant Control Using Integral Sliding Mode Strategy With Application to Flexible Spacecraft", *International Journal of Systems Science*, Vol.44, N0.12, 2013, pp. 2273-2286.

[50] Cieslak, J., Henry, D., and Zolghadri, A., "Fault Tolerant Flight Control: From Theory To Piloted Flight Simulator Experiments," *IET control theory & applications*, Vol. 4, No. 8, 2010, pp. 1451-1464.

[51] Cai, W. C., Liao, X. H., and Song, Y. D., "Indirect Robust Adaptive Fault-Tolerant Control For Attitude Tracking Of Spacecraft," *Journal of Guidance, Control, and Dynamics*, Vol. 31, No. 5, 2008, pp. 1456-1463.

[52] Karlgaard, C. D., "Robust Rendezvous Navigation In Elliptical Orbit," *Journal of Guidance, Control, and Dynamics*, Vol. 29, No. 2, 2006, pp. 495-499.